Targeted ablation of TRAF6 inhibits skeletal muscle wasting in mice

Pradyut K. Paul,[1] Sanjay K. Gupta,[1] Shephali Bhatnagar,[1] Siva K. Panguluri,[1] Bryant G. Darnay,[2] Yongwon Choi,[3] and Ashok Kumar[1]

[1]Anatomical Sciences and Neurobiology, University of Louisville School of Medicine, Louisville, KY 40202
[2]Department of Experimental Therapeutics, University of Texas MD Anderson Cancer Center, Houston, TX 77030
[3]Pathology and Laboratory Medicine, University of Pennsylvania School of Medicine, Philadelphia, PA 19104

Skeletal muscle wasting is a major human morbidity, and contributes to mortality in a variety of clinical settings, including denervation and cancer cachexia. In this study, we demonstrate that the expression level and autoubiquitination of tumor necrosis factor (α) receptor adaptor protein 6 (TRAF6), a protein involved in receptor-mediated activation of several signaling pathways, is enhanced in skeletal muscle during atrophy. Skeletal muscle–restricted depletion of TRAF6 rescues myofibril degradation and preserves muscle fiber size and strength upon denervation. TRAF6 mediates the activation of JNK1/2, p38 mitogen-activated protein kinase, adenosine monophosphate–activated protein kinase, and nuclear factor κB, and induces the expression of muscle-specific E3 ubiquitin ligases and autophagy-related molecules in skeletal muscle upon denervation. Inhibition of TRAF6 also preserves the orderly pattern of intermyofibrillar and subsarcolemmal mitochondria in denervated muscle. Moreover, depletion of TRAF6 prevents cancer cachexia in an experimental mouse model. This study unveils a novel mechanism of skeletal muscle atrophy and suggests that TRAF6 is an important therapeutic target to prevent skeletal muscle wasting.

Introduction

Skeletal muscle atrophy or wasting is a devastating complication of a large number of chronic disease states such as cancer, diabetes, chronic heart failure, and cystic fibrosis (Jackman and Kandarian, 2004). Besides a reduced survival rate, muscle atrophy is related to poor functional status and health-related quality of life during starvation, denervation, immobilization, aging, and numerous other conditions (Kandarian and Stevenson, 2002). Rapid atrophy occurs because of accelerated proteolysis leading to a loss of fiber cross-sectional area (CSA), protein content, and strength in skeletal muscle (Glass, 2003; Jackman and Kandarian, 2004).

Recent findings indicate that skeletal muscles respond to different types of atrophy conditions by activating a complex network of biochemical and transcriptional pathways, leading to the expression of a set of genes termed "atrogenes" (Glass, 2003; Cao et al., 2005). Many atrogenes are the components of ubiquitin–proteasome system that provides a mechanism for selective degradation of regulatory and structural proteins (Glass, 2005; Solomon and Goldberg, 1996; Lecker et al., 2006). Two E3 ubiquitin ligases, muscle RING-finger 1 (*MuRF1*) and muscle atrophy F-box (*MAFbx*; also called *Atrogin-1*), have now been identified that are highly up-regulated in several distinct models of skeletal muscle atrophy in both rodents and humans (Bodine et al., 2001; Gomes et al., 2001). Their catabolic role in skeletal muscle has been established by the finding that targeted deletion of *MAFbx* or *MuRF1* rescues atrophy in several conditions (Bodine et al., 2001; Gomes et al., 2001; Glass, 2010). In addition, it is now increasingly clear that the autophagy–lysosomal pathway also plays a crucial role in myofibril proteolysis in skeletal muscle (Sandri, 2010). Accumulating evidence

Correspondence to Ashok Kumar: ashok.kumar@louisville.edu

Abbreviations used in this paper: AMPK, AMP-activated protein kinase; CK, creatine kinase; CSA, cross-sectional area; EMSA, electrophoretic mobility shift assay; GA, gastrocnemius; GAPDH, glyceraldehyde 3-phosphate dehydrogenase; H&E, hematoxylin and eosin; IKK, I κB kinase; IRES, internal ribosome entry site; JNK, c-Jun N-terminal kinase; LLC, Lewis lung carcinoma; MCK, muscle CK; MEF, mouse embryonic fibroblast; MyHC, myosin heavy chain; NF-κB; nuclear factor κB; nNOS, neuronal nitric oxide synthase; QRT-PCR, quantitative real-time PCR; STZ, streptozotocin; TA, tibial anterior; TRAF, TNF receptor–associated factor; TWEAK, TNF-like weak inducer of apoptosis.

The Rockefeller University Press $30.00
J. Cell Biol. Vol. 191 No. 7 1395–1411
www.jcb.org/cgi/doi/10.1083/jcb.201006098

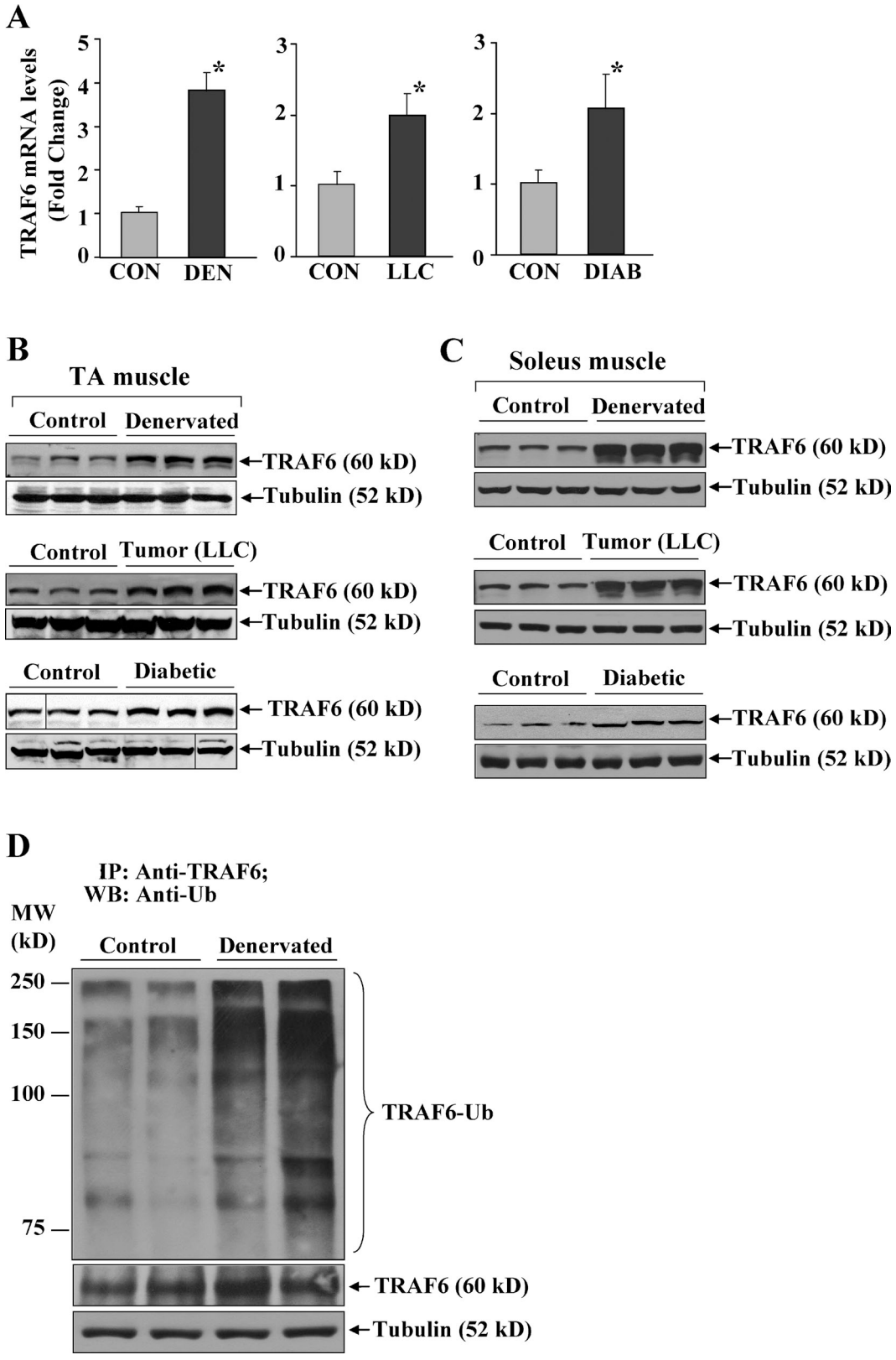

Figure 1. **Expression of TRAF6 is increased in atrophying skeletal muscle.** C57BL6 mice were subjected to either the conditions of denervation (sciatic nerve transection), tumor growth (LLC), or diabetes (STZ injection), and TA muscle was isolated and used for biochemical analyses. (A) Fold change in mRNA levels of TRAF6 in TA muscle of challenged mice compared with control mice. (B and C) Western blot analyses of protein levels of TRAF6 in TA muscle (B) and soleus muscle (C) of control and challenged mice. Black lines indicate that intervening lanes have been spliced out. (D) Control and denervated TA muscle extracts were immunoprecipitated with TRAF6 antibody followed by Western blotting using ubiquitin (Ub) antibody (top). Western blotting using anti-TRAF6 after stripping the membrane (middle) and anti-tubulin (bottom). Error bars indicate SD. *, $P < 0.01$ (values significantly different from controls). CON, control; DEN, denervated; DIAB, diabetic.

further indicates that these two pathways may function in a coordinated manner to augment protein degradation in different atrophy conditions (Mammucari et al., 2007; Zhao et al., 2007; Doyle et al., 2010).

Nuclear factor κB (NF-κB) is a proinflammatory transcription factor that regulates the expression of a large number of genes, including those involved in skeletal muscle proteolysis and fibrosis (Kumar et al., 2004). Increased activation of NF-κB has been consistently observed in skeletal muscle in different types of atrophy (Li et al., 2008). One of the important mechanisms by which NF-κB induces muscle atrophy is through upregulation of *MuRF1* (Cai et al., 2004; Mourkioti et al., 2006). In addition to NF-κB, several other signaling pathways have also been found to contribute to loss of skeletal muscle mass in catabolic conditions. Activation of p38 MAPK and AMP-activated protein kinase (AMPK) stimulates atrophy by augmenting the expression of *MAFbx* and *MuRF1* (Li et al., 2005; Krawiec et al., 2007; Romanello et al., 2010), whereas c-Jun N-terminal kinase (JNK) has been implicated in the activation of caspases in atrophying skeletal muscles (Supinski et al., 2009). Moreover, the activation of AMPK and NF-κB may also stimulate muscle proteolysis through enhancing the activity of autophagy–lysosomal system (Meley et al., 2006; Criollo et al., 2010a,b; Romanello et al., 2010). However, the proximal signaling events leading to the activation of various proteolytic systems in different types of atrophy remain enigmatic. It remains unknown whether the activation of various catabolic pathways is regulated through upstream activation of a common signaling network or if they are regulated through independent mechanisms in skeletal muscle in atrophy conditions.

TNF receptor–associated factors (TRAFs) comprise a family of conserved adaptor proteins involved in activation of various signaling cascades. Among known proteins of this family, TNF receptor adaptor protein 6 (TRAF6) has several distinct features that are not shared by other members of TRAF family (Lee and Lee, 2002; Chung et al., 2007). TRAF6 (along with TRAF2) is also an important E3 ubiquitin ligase, which in association with the dimeric ubiquitin-conjugating enzyme Ubc13/Uev1A promotes the unique Lys-63–linked poly-ubiquitin chains, rather than the conventional Lys-48–linked poly-ubiquitin chains that target proteins for degradation (Pickart, 2001; Lamothe et al., 2007a; Mukhopadhyay and Riezman, 2007). Studies in the recent past have established that TRAF6 is central to the activation of many signaling pathways including NF-κB, MAPK, and phosphatidylinositol 3-kinase (PI3K)/Akt in response to cytokines and microbial products (Chen, 2005; Lamothe et al., 2007a,b; Yamashita et al., 2008; Yang et al., 2009). Of note is the discovery that among all known TRAFs, only TRAF6 interacts with scaffold protein p62/Sequestosome 1, which is involved in regulation of autophagy and trafficking of proteins to the proteasome (Seibenhener et al., 2004; Wooten et al., 2005; Moscat et al., 2007; Nakamura et al., 2010). More recently, it has been found that TRAF6 promotes the Lys-63–linked ubiquitination of Beclin-1, which is critical for the induction of autophagy, in response to Toll-like receptor 4 signaling (Shi and Kehrl, 2010). Because many of these signaling pathways and proteolytic systems, activated through TRAF6-dependent mechanisms, are also activated in atrophying skeletal muscle, we hypothesize that TRAF6 plays a critical role in regulation of skeletal muscle mass in different catabolic conditions.

The major aim of this study was to investigate the physiological functions of TRAF6 in differentiated skeletal muscle and in catabolic conditions. Because conventional TRAF6-null mice die perinatally and neonatally because of severe osteoporosis and other defects (Lomaga et al., 1999; Naito et al., 1999; Kobayashi et al., 2003), for this study, we have generated skeletal muscle–specific TRAF6 knockout mice. Our results show that muscle-specific depletion of TRAF6 preserves skeletal muscle mass, fiber size, and contractile functions in response to denervation. Furthermore, specific inhibition of TRAF6 also inhibits skeletal muscle wasting in a mouse model of cancer cachexia.

Results

Expression of TRAF6 is increased in atrophying skeletal muscle

Although TRAF6 is expressed in several cell types, it remains unknown how the expression of TRAF6 is regulated in skeletal muscle cells. Using C2C12 myoblasts, we first studied how the levels of TRAF6 protein change at different time points after induction of differentiation. As shown in Fig. S1 A, TRAF6 is expressed in proliferating myoblasts, but its levels are dramatically reduced in differentiated myotubes. Reduced levels of TRAF6 protein appear to be a result of its reduced expression because transcript levels of TRAF6 were also significantly reduced in myotubes compared with myoblasts (Fig. S1 B). Interestingly, the expression of other TRAFs was not affected during myogenic differentiation (Fig. S1 A). Furthermore, TRAF6 is highly expressed in developing skeletal muscle of young animals but its levels are reduced in adult animals (Fig. S1 C).

We next determined whether the expression of TRAF6 changes in skeletal muscle in different atrophy conditions. As a model of denervation-induced muscle atrophy, C57BL6 mice were denervated for 4 d as described previously (Mittal et al., 2010). Lewis lung carcinoma (LLC) cells have been widely used to generate a model for cancer cachexia-induced muscle wasting in mice (Cai et al., 2004). To determine how expression of TRAF6 is regulated in cachexia, C57BL6 mice were given a single subcutaneous injection of LLC cells (in the left flank), which led to the growth of tumors at the site of injection. After 12 d of LLC inoculation, the right hind limb muscles were isolated and analyzed for TRAF6 expression. To induce type I diabetes, C57BL6 mice were treated with chronic intraperitoneal injections of streptozotocin (STZ) for 5 d as described previously (Baba et al., 2009). Finally, skeletal muscles of control and challenged mice were isolated and processed for studying mRNA and protein levels using quantitative real-time PCR (QRT-PCR) and Western blotting, respectively. As shown in Fig. 1 A, the mRNA levels of TRAF6 were significantly upregulated in tibial anterior (TA) muscle of mice subjected to denervation, cancer cachexia, or diabetes. Consistent with mRNA levels, the protein levels of TRAF6 were also found to be increased in TA (contains predominantly fast-type fiber) and

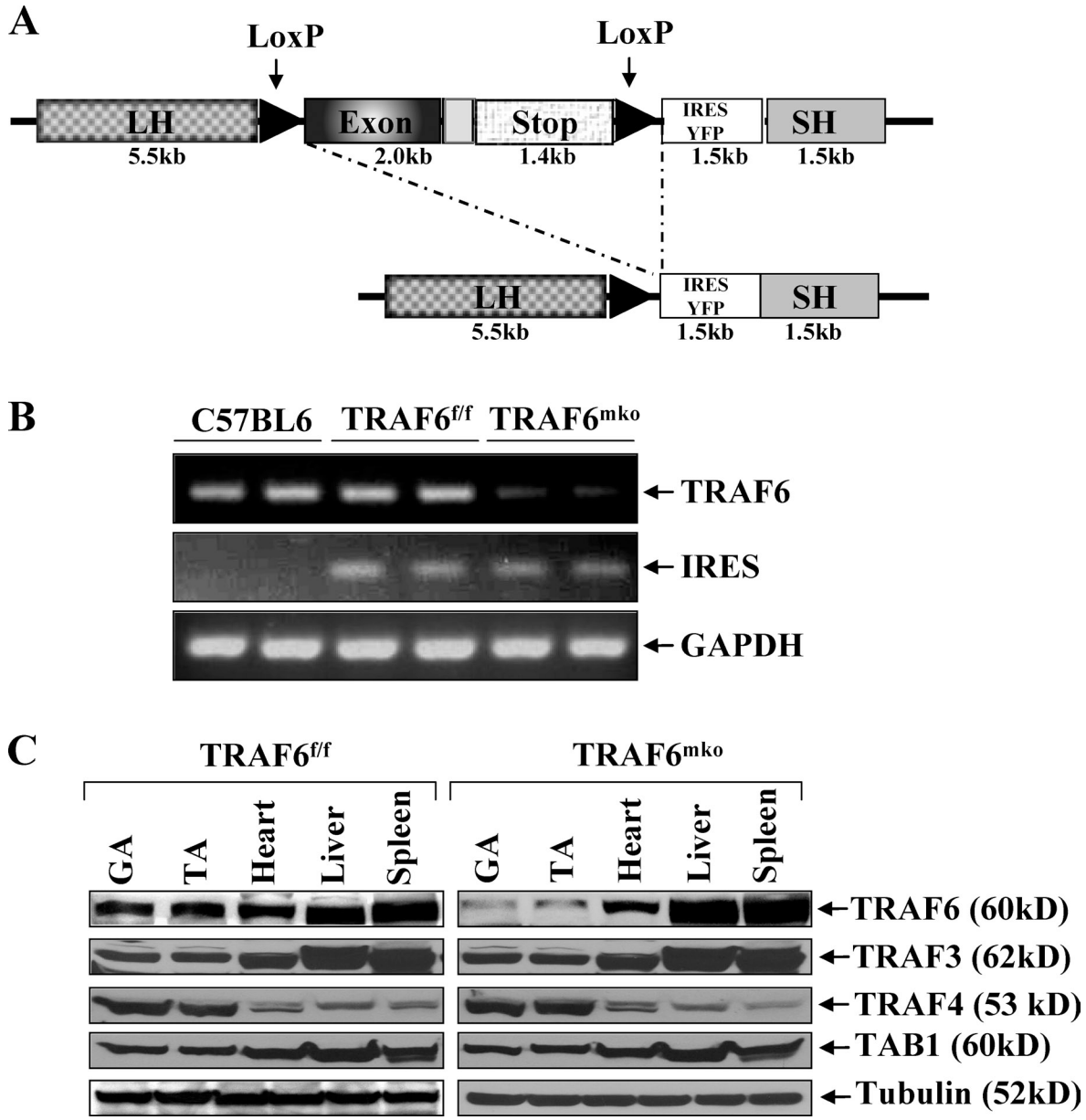

Figure 2. **Generation of skeletal muscle–specific TRAF6 knockout mice.** (A) Strategy for the generation of TRAF6^{mko} mice. TRAF6$^{f/f}$ mice were generated by homologous recombination of a 15-kb DNA fragment containing a 5.5-kb-long homologous (LH) fragment, loxP site, 2-kb TRAF6 exon, 1.4-kb stop cassette, loxP site, 1.5-kb IRES-YFP, and 1.5-kb short homologous (SH) fragment. These mice were crossed with MCK-Cre mice to delete the floxed exon. (B) Representative photomicrographs of the semiquantitative reverse polymerase PCR gels showing reduced expression of TRAF6 in TA muscle of TRAF6^{mko} mice compared with TRAF6$^{f/f}$ or C57BL6 mice. The levels of IRES and GAPDH were comparable between TRAF6$^{f/f}$ and TRAF6^{mko} mice. (C) Western blot analysis of TRAF6, TRAF3, TRAF4, TAB1, and tubulin protein levels showed depletion of TRAF6 only in skeletal muscle of TRAF6^{mko} mice.

soleus (contains both slow- and fast-type fibers) in all the three models of atrophy studied (Fig. 1, B and C).

Because TRAF6 is an E3 ubiquitin ligase that undergoes lysine-63–linked autoubiquitination in response to cytokines and microbial products (Lamothe et al., 2007a,b), we also investigated whether TRAF6 is ubiquitinated in skeletal muscle under the conditions of atrophy. Protein extracts prepared from control, and denervated TA muscles were immunoprecipitated with TRAF6 antibody followed by Western blotting using ubiquitin antibody. A marked increase in ubiquitinated TRAF6 protein was noticeable in denervated skeletal muscle compared with control muscle (Fig. 1 D). These observations suggest that expression and autoubiquitination of TRAF6 are stimulated in skeletal muscle in settings of atrophy.

Muscle-specific depletion of TRAF6 does not cause any overt phenotype in mice

To investigate the role of TRAF6 in skeletal muscle, we developed a conditional TRAF6 gene inactivation strategy based on the Cre–LoxP system. TRAF6$^{flox/flox}$ (TRAF6$^{f/f}$) mice were crossed with muscle creatine kinase (MCK)-Cre mice in which Cre-mediated recombination occurs in postmitotic myofibers but not in satellite cells (Brüning et al., 1998). The design of targeting construct to generate muscle-specific TRAF6 knockout (TRAF6^{mko} henceforth)

mice is described in Fig. 2 A and in a published article (Kobayashi et al., 2003). The breeding strategy for generation of TRAF6^{mko} and littermate TRAF6$^{f/f}$ mice is depicted in Fig. S2 A. Depletion of TRAF6 in skeletal muscle tissues was assessed by semiquantitative reverse-transcription PCR using TRAF6 exon 7, internal ribosome entry site (IRES), and glyceraldehyde 3-phosphate dehydrogenase (GAPDH) primers. A significant reduction in TRAF6 transcript levels in skeletal muscle was noticeable in TRAF6^{mko} mice, whereas levels of IRES and GAPDH were comparable between C57BL6 (wild-type), TRAF6$^{f/f}$, and TRAF6^{mko} mice (Fig. 2 B). By performing Western blotting, we also measured protein levels of TRAF6 in skeletal muscle and other tissues of 6-wk-old TRAF6$^{f/f}$ and TRAF6^{mko} mice. As shown in Fig. 2 C, the protein levels of TRAF6 were considerably reduced in gastrocnemius (GA) and TA muscle of TRAF6^{mko} compared with TRAF6$^{f/f}$ mice. There was no major difference in the levels of TRAF6 in other tissues (e.g., heart, liver, and spleen). Furthermore, the expression of some other TRAFs (e.g., TRAF3 and TRAF4) and an adapter protein TAB1 did not change in skeletal muscle and other tissues of TRAF6^{mko} and TRAF6$^{f/f}$ mice, which indicated depletion of TRAF6 specifically in skeletal muscle of TRAF6^{mko} mice (Fig. 2 C).

TRAF6^{mko} pups were viable, born in the expected Mendelian ratio, and indistinguishable from their littermate TRAF6$^{f/f}$ mice. There was no significant difference in overall body weight or individual muscle tissue weights between littermate TRAF6$^{f/f}$ and TRAF6^{mko} mice (unpublished data). At the age of 10 d (young) and 8 wk (adult), we analyzed muscle tissues of TRAF6$^{f/f}$ and TRAF6^{mko} mice. Hematoxylin and eosin (H&E) staining of muscle section and histomorphometric analysis showed that the fiber CSA was comparable in TRAF6$^{f/f}$ and TRAF6^{mko} mice (Fig. S2, B and C). Depletion of TRAF6 in skeletal muscle did not affect the count of fibers per unit area in young or adult mice (Fig. S2 D).

Measurement of serum levels of creatine kinase (CK) in TRAF6$^{f/f}$ and TRAF6^{mko} mice showed no significant difference, which suggests that depletion of TRAF6 does not cause any overt myopathy in mice (Fig. S3 A). We also investigated whether TRAF6 regulates the composition of oxidative (type I, slow-type) and glycolytic (type II, fast-type) fibers in skeletal muscle of mice. Staining of soleus muscle section with both anti–myosin heavy chain (MyHC) type I and anti-MyHC type II followed by counting of each type of fiber showed that depletion of TRAF6 does not affect fiber composition in skeletal muscle of mice (Fig. S3 B). Finally, we also found that specific muscle force produced in isometric contractions was similar in TRAF6$^{f/f}$ and TRAF6^{mko} mice (Fig. S3 C). These observations suggest that TRAF6 depletion does not produce any overt phenotype in differentiated muscle of mice.

Depletion of TRAF6 rescues denervation-induced muscle atrophy

Left hind limb muscles of 3-mo-old TRAF6$^{f/f}$ and TRAF6^{mko} mice were denervated by transecting sciatic nerve, whereas the right hind limb was sham-operated. Gross analyses 14 d after denervation showed that the loss of GA muscle was considerably reduced in TRAF6^{mko} mice compared with TRAF6$^{f/f}$ mice (Fig. 3 A). We also measured wet weights of different muscles (soleus, TA, and GA) from tendon to tendon. Interestingly, denervation-induced loss of soleus, TA, and GA muscle weight was significantly rescued in TRAF6^{mko} compared with TRAF6$^{f/f}$ mice (Fig. 3 B). We next performed H&E staining on TA and soleus muscle sections of control and denervated TRAF6$^{f/f}$ and TRAF6^{mko} mice and quantified fiber CSA. Interestingly, fiber CSA was significantly preserved in TA (Figs. 3, C and D) and soleus (Figs. 3, E and F) muscle of TRAF6^{mko} mice compared with littermate TRAF6$^{f/f}$ mice upon denervation. Furthermore, force production in isometric contraction was significantly higher in denervated soleus muscle of TRAF6^{mko} mice compared with TRAF6$^{f/f}$ mice (Fig. 3 G).

Inhibition of TARF6 prevents proteolysis in denervated skeletal muscle

Skeletal muscle atrophy can occur due to enhanced proteolysis, reduced protein synthesis, or both (Jackman and Kandarian, 2004; Glass, 2005). We investigated the possibility of whether TRAF6 affects myofibril proteolysis or if it represses expression of specific muscle proteins in denervated skeletal muscle. Sham-operated or denervated TA muscles were isolated from TRAF6$^{f/f}$ and TRAF6^{mko} mice, and muscle extracts made were used to measure the levels of specific muscle proteins by Western blotting. As shown in Fig. 4 A, the levels of MyHCs were considerably reduced in denervated TA muscle compared with sham-operated TRAF6$^{f/f}$ mice. Interestingly, the denervation-induced loss of MyHC was rescued in TRAF6^{mko} mice (Fig. 4 A). Quantification of band intensities from immunoblots confirmed that the levels of MyHC were significantly higher in denervated TA muscle of TRAF6^{mko} mice compared with TRAF6$^{f/f}$ mice (Fig. 4 B). Consistent with a previously published study (Matsuda et al., 1984), we found that the protein levels of tropomyosin were increased in denervated muscle, though there was no major difference in the levels of tropomyosin in denervated muscle of TRAF6^{mko} mice compared with TRAF6$^{f/f}$ mice (Fig. 4 A). We also did not find any significant difference in the levels of many other muscle proteins such as troponin, neuronal nitric oxide synthase (nNOS), laminin, β-dystroglycan, dystrophin, utrophin, and sarcomeric α-actin in control and denervated skeletal muscle of TRAF6$^{f/f}$ and TRAF6^{mko} (Fig. 4 A). These data are in agreement with previously published findings that muscle wasting involves degradation of only select muscle proteins (Acharyya et al., 2004; Mittal et al., 2010).

To further determine whether increased levels of MyHC in denervated skeletal muscle of TRAF6^{mko} compared with TRAF6$^{f/f}$ mice were a result of its reduced degradation or increased expression, we measured mRNA levels by QRT-PCR. Interestingly, there was no significant difference between mRNA levels of MyHC between control and denervated TA muscle of TRAF6$^{f/f}$ and TRAF6^{mko} mice (Fig. 4 C). Collectively, these results indicate that the inhibition of TRAF6 prevents the proteolytic degradation of MyHC without affecting its expression in denervated skeletal muscles.

TRAF6 is required for the activation of ubiquitin–proteasome and autophagy systems in denervated skeletal muscles

The ubiquitin–proteasome system is the major pathway that causes the degradation of muscle proteins in various atrophying

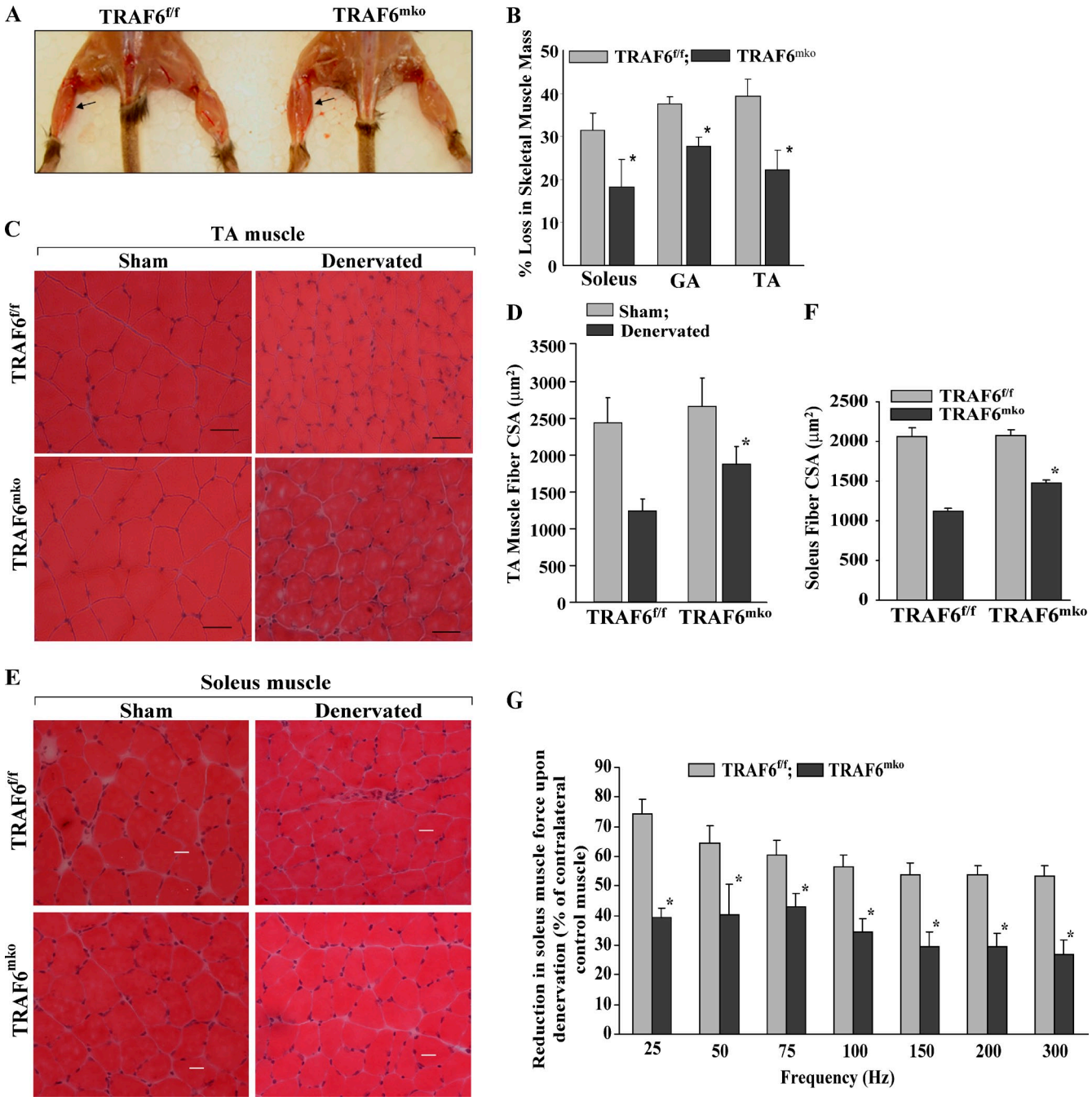

Figure 3. **Ablation of TRAF6 prevents denervation-induced muscle loss in mice.** 3-mo-old TRAF6$^{f/f}$ and TRAF6^{mko} mice were denervated by transection of sciatic nerve. (A) Arrows point to GA muscle 14 d after denervation. (B) TA, GA, and soleus muscle were isolated tendon to tendon from TRAF6$^{f/f}$ and TRAF6^{mko} mice 14 d after denervation (n = 8 per group), and their wet weight was measured. (C) H&E-stained sections of TA muscle of TRAF6$^{f/f}$ and TRAF6^{mko} mice 14 d after denervation. Bars, 50 µm. (D) Quantification of mean fiber CSA of TA muscle in TRAF6$^{f/f}$ and TRAF6^{mko} mice 14 d after denervation (n = 8 in each group). (E) Representative H&E-stained sections of soleus muscle of TRAF6$^{f/f}$ and TRAF6^{mko} mice. Bars, 20 µm. (F) Quantification of fiber CSA in soleus muscle in TRAF6$^{f/f}$ and TRAF6^{mko} mice after denervation (n = 8 in each group). (G) Denervation-induced loss in absolute muscle force production in isometric contraction was measured in soleus muscle of TRAF6$^{f/f}$ (n = 4) and TRAF6^{mko} (n = 4) mice at the indicated frequencies. Error bars represent SD. *, $P < 0.05$ (values significantly different from denervated muscle of TRAF6$^{f/f}$ mice).

conditions (Solomon and Goldberg, 1996; Cao et al., 2005). Previous studies have reported enhanced expression of several components of the ubiquitin–proteasome system and an increase in the amounts of ubiquitinated proteins in different muscle-wasting conditions, including denervation (Solomon and Goldberg, 1996; Cao et al., 2005). Among several markers of muscle atrophy, two atrogenes, MAFbx/Atrogin-1 and MuRF1, have been found to be highly expressed in atrophying muscles (Bodine et al., 2001; Gomes et al., 2001). To determine whether TRAF6 is involved in expression of MAFbx and MuRF1, we measured their transcript levels in denervated skeletal muscle using QRT-PCR technique. In agreement with published reports (Bodine et al., 2001; Gomes et al., 2001), mRNA levels of both MAFbx and MuRF1 were found to be drastically increased in

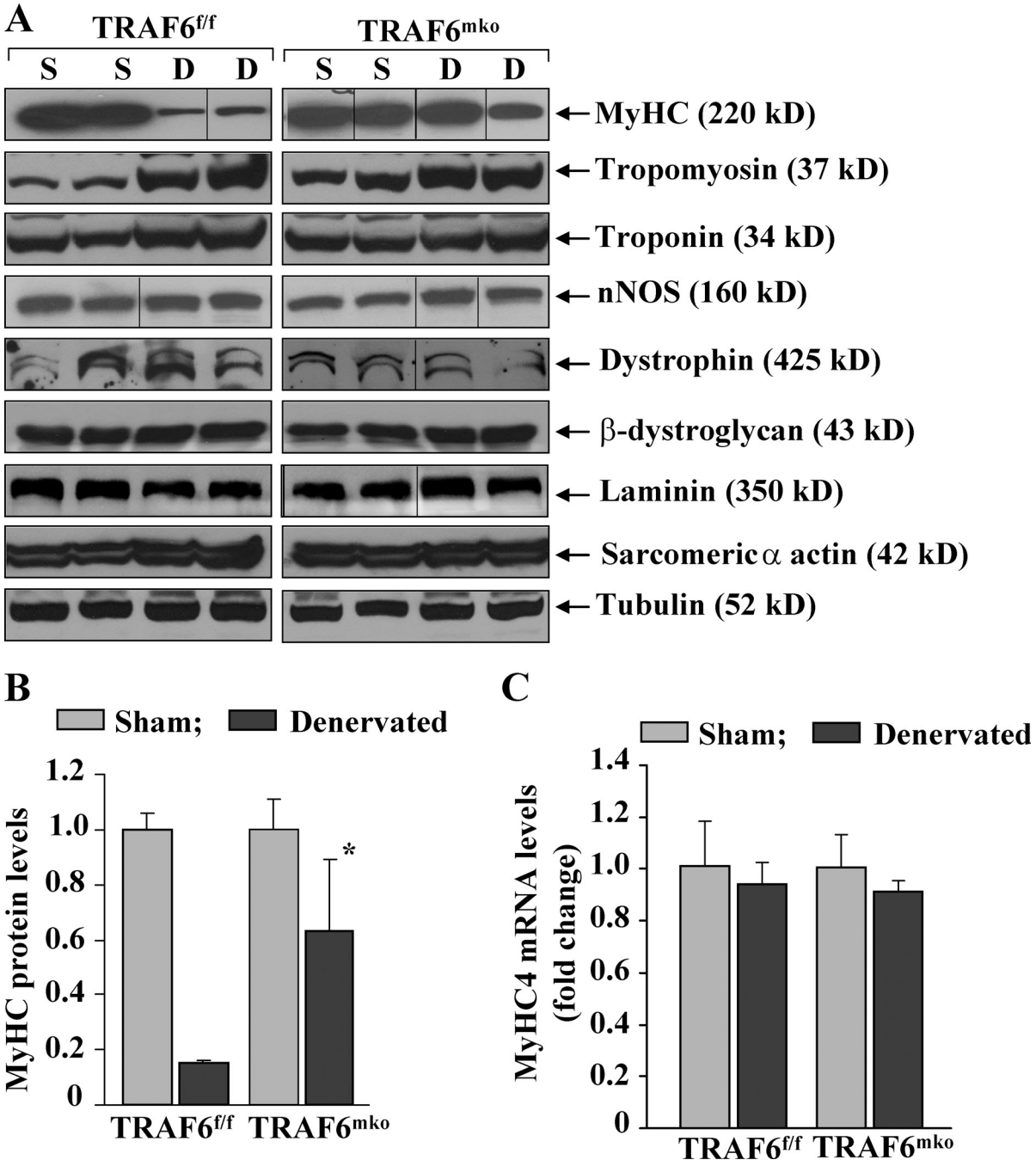

Figure 4. **Depletion of TRAF6 prevents degradation of specific muscle proteins in denervated skeletal muscle.** (A) Representative immunoblots for MyHC, tropomyosin, troponin, nNOS, dystrophin, β-dystroglycan, sarcomeric α-actin, laminin, and tubulin in TA muscle 10 d after denervation. Black lines indicate that intervening lanes have been spliced out. (B) Fold change in protein levels of MyHC in TA muscle of $TRAF6^{f/f}$ ($n = 4$) and $TRAF6^{mko}$ ($n = 4$) mice after denervation. (C) Fold change in mRNA level of MyHC in TA muscle of $TRAF6^{f/f}$ ($n = 4$) and $TRAF6^{mko}$ ($n = 4$) mice upon denervation. Error bars represent SD. *, $P < 0.05$ (values significantly different from $TRAF6^{f/f}$ mice). Black lines indicate that intervening lanes have been spliced out.

denervated TA muscles compared with sham-injured control muscle (Fig. 5 A). Interestingly, mRNA levels of MAFbx and MuRF1 were significantly down-regulated in denervated muscle of $TRAF6^{mko}$ mice compared with $TRAF6^{f/f}$, which suggests that TRAF6 regulates the expression of these two atrogenes in denervated skeletal muscle (Fig. 5 A).

Accumulating evidence suggests that autophagy–lysosome-mediated proteolysis also contributes to degradation of muscle protein during atrophy (Zhao et al., 2007; Sandri, 2010). We next sought to determine whether TRAF6 affects autophagy in denervated skeletal muscle. To answer this question, we compared the mRNA levels of major autophagy-related genes *LC3B*, *Beclin1*, and *Gabarapl1*, which are reported to be significantly up-regulated in denervated muscles (Zhao et al., 2007). Our results showed that the mRNA levels of *LC3B*, *Beclin1*, and *Gabarapl1* were significantly reduced in denervated skeletal muscle of $TRAF6^{mko}$ mice compared with $TRAF6^{f/f}$ mice (Fig. 5 B). In agreement with their mRNA levels, the protein levels of

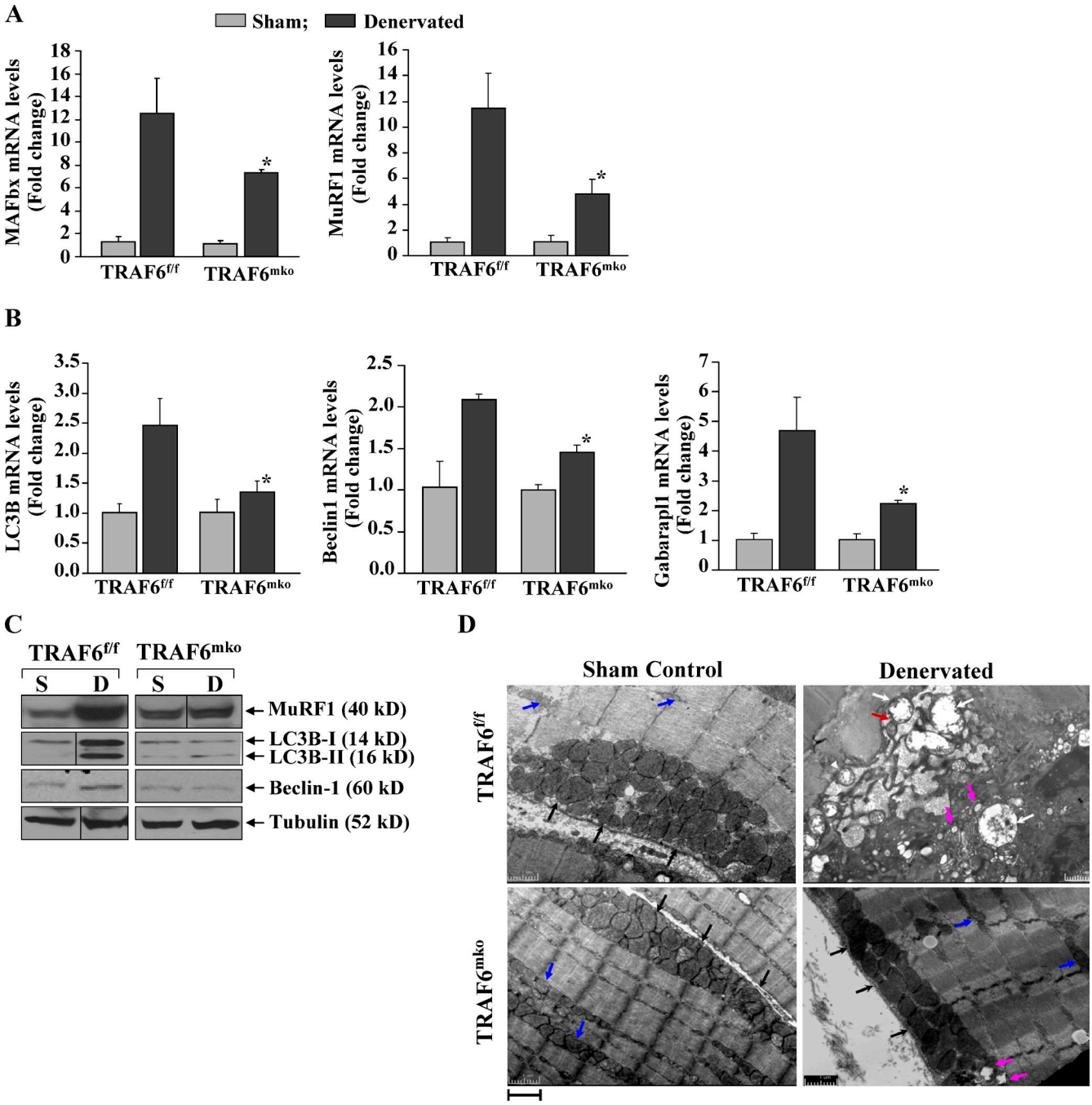

Figure 5. **TRAF6 is required for the activation of the ubiquitin–proteasome and autophagy systems in denervated skeletal muscle.** 3-mo-old TRAF6$^{f/f}$ and TRAF6^{mko} mice were subjected to denervation for 10 d, and TA muscles were isolated for biochemical analyses. (A) Transcript levels of MAFbx and MuRF1 (measured by QRT-PCR assays) were significantly lower in denervated TA muscle of TRAF6^{mko} mice compared with TRAF6$^{f/f}$ mice. (B) The expression levels of autophagy-related genes LC3B, Beclin1, and Gabarapl1 were also significantly reduced in denervated TA muscle of TRAF6^{mko} mice compared with TRAF6$^{f/f}$ mice. Error bars represent SD. *, $P < 0.05$ (values significantly different from those of denervated TA muscle of TRAF6$^{f/f}$ mice). (C) Representative immunoblots presented here demonstrate reduced protein levels of MuRF1, LC3B, and Beclin1 in denervated TA muscle of TRAF6^{mko} mice compared with TRAF6$^{f/f}$ mice. Black lines indicate that intervening lanes have been spliced out. (D) Analyses of longitudinal sections of control and denervated TA muscle of TRAF6$^{f/f}$ and TRAF6^{mko} mice using transmission electron microscopy. Black arrows point to subsarcolemmal mitochondrial distribution, blue arrows point to intermyofibrillar mitochondria, white arrows point to autophagosomes, pink arrows point to autophagic vacuoles, and red arrows point to mitochondria being engulfed by autophagosome. Bar, 1 µm.

MuRF1, LC3B, and Beclin1 were also found to be reduced in denervated muscle of TRAF6^{mko} compared with TRAF6$^{f/f}$ mice (Fig. 5 C).

To further ascertain whether depletion of TRAF6 rescues autophagy, we analyzed control and denervated skeletal muscle of TRAF6$^{f/f}$ and TRAF6^{mko} mice by transmission electron microscopy. As shown in Fig. 5 D, sham-operated skeletal muscle of both TRAF6$^{f/f}$ and TRAF6^{mko} mice contained well-organized myofibrillar structure, and normal subsarcolemmal and intermyofibrillar distribution of mitochondria (indicated by black

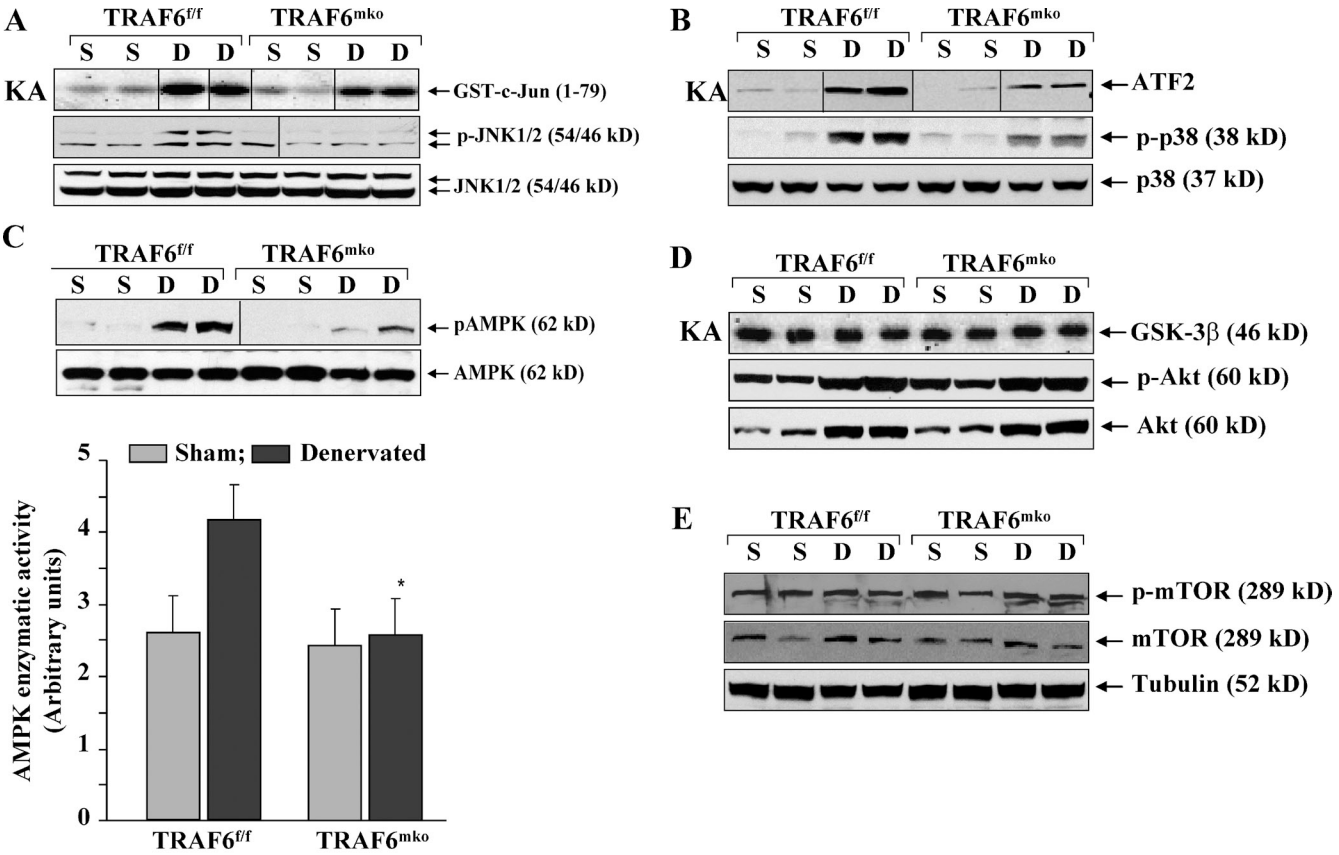

Figure 6. **Activation of different signaling proteins in denervated muscle of TRAF6$^{f/f}$ and TRAF6^{mko} mice.** Protein extracts prepared from control or 7-d post-denervated muscle of TRAF6$^{f/f}$ and TRAF6^{mko} mice were used for in vitro kinase assays or Western blotting. (A) Representative gel pictures show kinase activity, and phosphorylated and total JNK1/2 protein levels in control and denervated TA muscle of TRAF6^{mko} and TRAF6$^{f/f}$ mice. (B) Kinase activity and phosphorylated and total p38 MAPK levels in TA muscle of TRAF6^{mko} and TRAF6$^{f/f}$ mice. (C) Gel pictures showing levels of phosphorylated and total AMPK protein in TA muscle of TRAF6^{mko} and TRAF6$^{f/f}$ mice (top). Kinase activity of AMPK (bottom) was measured using a commercially available kit. Error bars represent SD. *, $P < 0.05$ (values significantly different from those of denervated TA muscle of TRAF6$^{f/f}$ mice). Black lines indicate that intervening lanes have been spliced out. (D) Kinase activity and phosphorylated and total Akt protein levels in TA muscle of TRAF6^{mko} and TRAF6$^{f/f}$ mice. (E) Phosphorylated and total mTOR protein levels in TA muscle of TRAF6^{mko} and TRAF6$^{f/f}$ mice. D, denervated; KA, kinase assay; S, sham operated.

and blue arrows), with no evidence of autophagosome formation. In contrast, denervated muscle of TRAF6$^{f/f}$ mice showed disorganization of mitochondria in intermyofibrillar as well as subsarcolemmal space and a drastic increase in autophagic vacuole formation (Fig. 5 D, white arrows) and fusion of mitochondria with autophagosome membrane (red arrows). Interestingly, all these characteristics of muscle atrophy and autophagy were considerably reduced in denervated muscle of TRAF6^{mko} mice (Fig. 5 D). Collectively, these results suggest that TRAF6 is involved in the activation of both ubiquitin–proteasome and autophagy systems in denervated skeletal muscle.

TRAF6 mediates the activation of JNK, p38 MAPK, and AMPK in denervated skeletal muscle

Recent findings have identified several signaling pathways that regulate skeletal muscle mass in both hypertrophy and atrophy conditions (Glass, 2005, 2010). Because TRAF6 is a major adaptor protein involved in activation of various cell signaling pathways, we next investigated whether TRAF6 functions through the activation of specific signaling proteins in atrophying skeletal muscle. Control and denervated TA muscle from TRAF6$^{f/f}$ and TRAF6^{mko} mice were isolated, and muscle extracts were analyzed by in vitro kinase assays and Western blotting using antibodies that determine phosphorylated or total levels of specific proteins. Our results showed that denervation augments the kinase activity and phosphorylation of JNK1/2 (Fig. 6 A) and p38 MAPK (Fig. 6 B) in skeletal muscle of mice. Importantly, we found that the depletion of TRAF6 was sufficient to block the activation of JNK1/2 (fold change in kinase activity: TRAF6$^{f/f}$, 15.83 ± 0.41, vs. TRAF6^{mko}, 12.11 ± 0.10) and p38 MAPK (fold change in kinase activity: TRAF6$^{f/f}$, 10.76 ± 0.74, vs. TRAF6^{mko}, 7.31 ± 0.40) in denervated muscles. In addition, we also found that the phosphorylation of AMPK as well as its kinase activity were significantly inhibited (fold change in kinase activity: TRAF6$^{f/f}$, 4.15 ± 0.24, vs. TRAF6^{mko}, 2.57 ± 0.39) in denervated skeletal muscle of TRAF6^{mko} compared with TRAF6$^{f/f}$ mice (Fig. 6 C). Because JNK, p38 MAPK, and AMPK are linked with skeletal muscle atrophy (Li et al., 2005; Supinski et al., 2009; Romanello et al., 2010), their reduced activation in denervated skeletal muscle of TRAF6^{mko} suggests that TRAF6 might be mediating skeletal muscle atrophy through the downstream activation of these kinases in response to denervation.

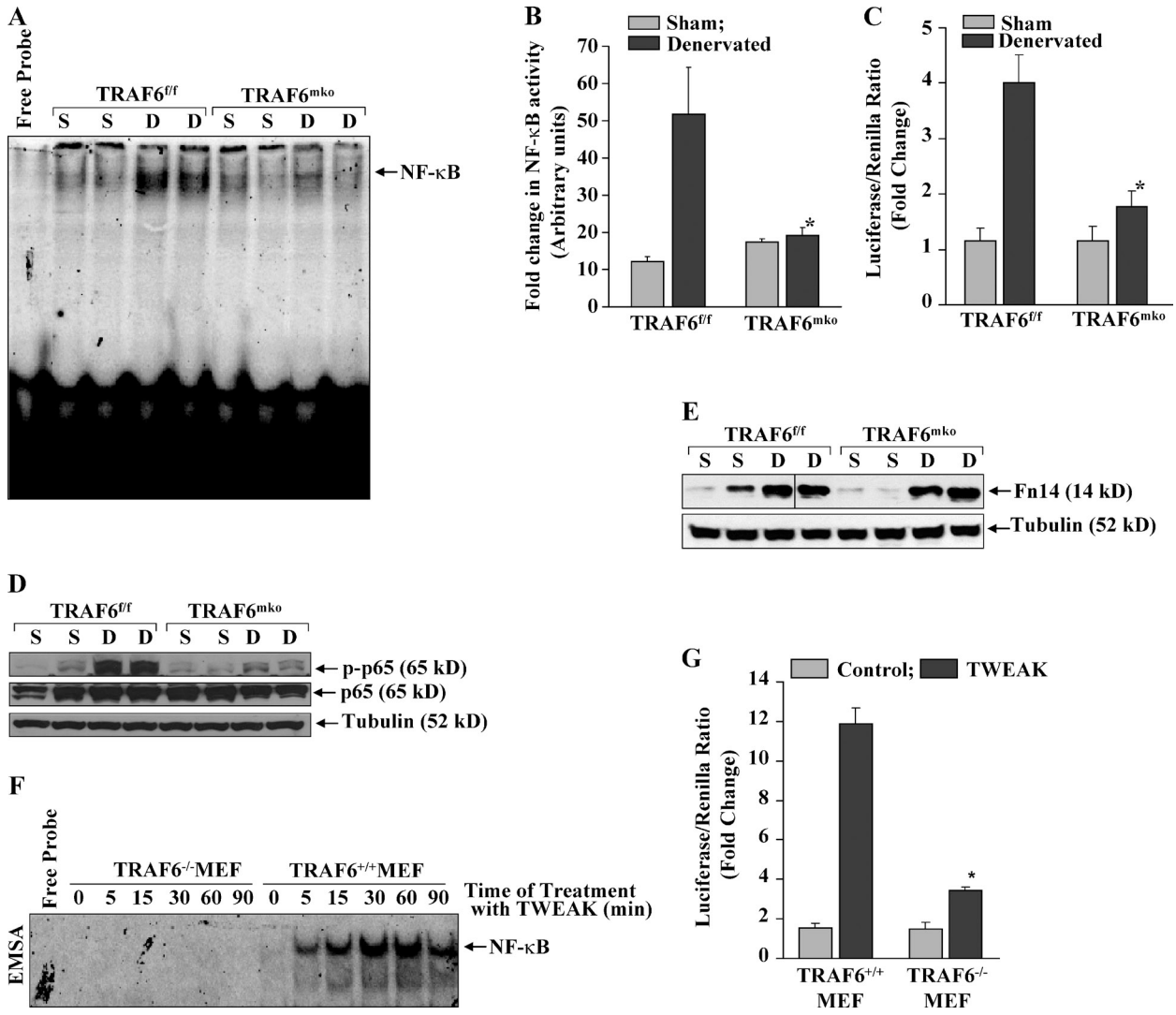

Figure 7. **TRAF6 is required for the activation of NF-κB transcription factor in denervated skeletal muscle.** (A) DNA-binding activity of NF-κB measured by EMSA in TA muscle of TRAF6$^{f/f}$ and TRAF6^{mko} mice 10 d after denervation. A representative EMSA gel from three independent experiments is presented. (B) Quantification of fold change in DNA-binding activity of NF-κB in TA muscle of TRAF6$^{f/f}$ (n = 6) and TRAF6^{mko} (n = 6) mice. (C) Fold change in NF-κB reporter gene activity (normalized using Renilla luciferase) in TA muscle of TRAF6$^{f/f}$ and TRAF6^{mko} mice in response to denervation. (D) Western blot analyses of the phosphorylated and total form of p65 protein in TA muscle of TRAF6$^{f/f}$ and TRAF6^{mko} mice. (E) Western blot analysis of Fn14 protein in TA muscle of TRAF6$^{f/f}$ and TRAF6^{mko} mice 4 d after denervation. (F) TRAF6$^{+/+}$ and TRAF6$^{-/-}$ MEF were treated with 100 ng/ml TWEAK for the indicated time intervals, and the activation of NF-κB was studied by EMSA. A representative EMSA gel from two independent experiments is presented. (G) Fold change in NF-κB reporter gene activity (normalized using Renilla luciferase) in TRAF6$^{+/+}$ and TRAF6$^{-/-}$ MEFs measured after 24 h of 100 ng/ml TWEAK treatment. Error bars represent SD. D, denervated; S, sham-operated. *, P < 0.01 (values significantly different from denervated TA muscle of TRAF6$^{f/f}$ mice).

Interestingly, levels of kinase activity and/or phosphorylation of Akt and mTOR, which are involved in anabolic pathways (Glass, 2005, 2010), were similar in denervated muscle of TRAF6$^{f/f}$ and TRAF6^{mko} mice (Fig. 6, D and E). These results suggest that TRAF6 mediates the activation of selective pathways, especially those involved in catabolic mechanisms in denervated muscles.

TRAF6 is involved in denervation-induced activation of NF-κB in skeletal muscle

Accumulating evidence suggests that NF-κB is a major transcription factor, the activation of which causes severe muscle wasting in response to diverse stimuli (Li et al., 2008). We investigated whether TRAF6 plays a role in activation of NF-κB in denervated skeletal muscle. Sham and denervated TA muscle were isolated from TRAF6$^{f/f}$ and TRAF6^{mko} mice, and nuclear extracts were analyzed for NF-κB activity by an electrophoretic mobility shift assay (EMSA). The denervation-induced activation of NF-κB in skeletal muscle was inhibited in TRAF6^{mko} mice compared with TRAF6$^{f/f}$ mice (Fig. 7, A and B). Furthermore, transcriptional activation of NF-κB measured after electroporating an NF-κB reporter plasmid (Fig. 7 C) and the levels of phosphorylation of NF-κB subunit p65 (Fig. 7 D) were also significantly inhibited in denervated muscle of TRAF6^{mko} mice compared with TRAF6$^{f/f}$ mice. This suggests that TRAF6 is required for the activation of NF-κB upon denervation.

We have recently reported that TNF-like weak inducer of apoptosis (TWEAK) cytokine is a major mediator of

denervation-induced skeletal muscle atrophy in mice (Mittal et al., 2010). Normal skeletal muscle expresses TWEAK but not its receptor Fn14. However, in response to denervation, the expression of Fn14 goes up dramatically; this allows for TWEAK activation of NF-κB (Mittal et al., 2010). We first investigated whether TRAF6 regulates the expression of Fn14 in response to denervation. No major difference was noticed in Fn14 protein levels between $TRAF6^{f/f}$ and $TRAF6^{mko}$ mice upon denervation (Fig. 7 E). We next asked whether TRAF6 is involved in TWEAK-induced activation of NF-κB. To answer this question, we used TRAF6-deficient mouse embryonic fibroblasts (MEFs). Interestingly, TWEAK-induced increases in DNA-binding activity (Fig. 7 F) and transcriptional activation of NF-κB (Fig. 7 G) were significantly inhibited in $TRAF6^{-/-}$ MEFs compared with $TRAF6^{+/+}$, which indicates that TRAF6 is required for the activation of NF-κB in response to TWEAK.

Depletion of TRAF6 prevents skeletal muscle wasting in response to tumor growth

Tissue loss is a common consequence in cancer cachexia (Acharyya and Guttridge, 2007). To understand whether TRAF6 plays any role in cancer cachexia and subsequent muscle loss, $TRAF6^{mko}$ and $TRAF6^{f/f}$ mice were injected with LLC cells in the left flank. Although no significant difference was observed in tumor growth in these two mice, skeletal muscle of $TRAF6^{f/f}$ mice showed a significant reduction in fiber CSA 14 d after inoculation with LLC cells (Fig. 8, A and B). Surprisingly, fiber CSA in LLC-bearing $TRAF6^{mko}$ mice was almost completely preserved, which indicates that the TRAF6 mediates the loss of muscle mass in response to tumor growth (Fig. 8 B). Though the molecular basis of cachexia is not yet fully resolved, a majority of factors that induce cachexia involve the activation of NF-κB at the distal end of their signaling cascade (Li et al., 2008). This has been corroborated by the finding that the inhibition of NF-κB prevents tumor-induced muscle loss in mice (Cai et al., 2004). We investigated whether TRAF6 functions through the activation of NF-κB in this model of cancer cachexia. Our results showed a significant inhibition in DNA-binding activity of NF-κB in skeletal muscle of LLC-bearing $TRAF6^{mko}$ mice compared with $TRAF6^{f/f}$ mice (Fig. 8 C). Furthermore, the expression of *MuRF1*, *LC3B*, and *Beclin1* was blocked in LLC-injected $TRAF6^{mko}$ compared with $TRAF6^{f/f}$ mice; this indicates that, similar to denervation, inhibition of TRAF6 prevents tumor-induced activation of ubiquitin–proteasome and autophagy–lysosomal systems in skeletal muscle (Fig. 8 D).

Discussion

The results of the present study indicate a novel role of TRAF6, formerly known as an E3 ubiquitin ligase with involvement in several signaling pathways, in upstream regulation of muscle atrophy. More recently, understanding about the intracellular signaling pathways governing skeletal muscle mass in response to both atrophy and hypertrophy stimuli has taken a quantum leap, though most of the recent investigations were focused on studying the role of various effector kinases and downstream transcription factors (Li et al., 2005; Krawiec et al., 2007; Supinski et al., 2009; Glass, 2010; Romanello et al., 2010). The initial events that trigger the activation of one or multiple signaling pathways in the conditions of atrophy or hypertrophy remain poorly defined. Our study has identified TRAF6 as a major upstream regulator of skeletal muscle atrophy in response to both physiological (e.g., denervation) and pathological (e.g., cancer cachexia) stimuli. Although it remains unknown what elicits the expression and autoubiquitination of TRAF6 in atrophying muscle, it was of interest to note that proliferating myoblasts express high levels of TRAF6, which is considerably reduced after their differentiation into myotubes (Fig. S1). Therefore, it appears that the reduced expression of TRAF6 in differentiated muscle could be a mechanism to prevent the activation of various catabolic pathways under normal conditions. In contrast, elevated levels of TRAF6 in undifferentiated myoblasts or in skeletal muscle of young animals is consistent with published findings that TRAF6 may be required for the proliferation and differentiation of muscle progenitor cells during skeletal muscle development (Chung et al., 2007; Zapata et al., 2007).

Skeletal muscle atrophy, in different catabolic conditions, involves the downstream activation of the ATP-dependent ubiquitin–proteasome system (Solomon and Goldberg, 1996). It has been found that in almost all muscle-wasting conditions, the expression of two muscle-specific E3 ubiquitin ligases, *MAFbx* and *MuRF1*, which label the target proteins for degradation by 26S proteasome, is highly up-regulated (Bodine et al., 2001; Gomes et al., 2001; Cao et al., 2005). Moreover, a few substrates that *MAFbx* and *MuRF1* target in atrophying skeletal muscle have now been identified (Kedar et al., 2004; Tintignac et al., 2005; Clarke et al., 2007, 2009). The present study suggests that one of the mechanisms by which TRAF6 induces degradation of muscle protein is through augmenting the expression of both *MAFbx* and *MuRF1* in denervated skeletal muscle (Fig. 5 A). Furthermore, our results demonstrating that the degradation of MyHC is significantly blocked in denervated skeletal muscle of $TRAF6^{mko}$ mice (Fig. 4) are in agreement with recent reports that *MuRF1* targets thick filament proteins including MyHC in skeletal muscle (Clarke et al., 2007; Cohen et al., 2009).

Although the exact mechanisms by which TRAF6 augments the expression of *MAFbx* and *MuRF1* are not clear, it has been consistently observed that the activity of TRAF6 is stimulated in response to many receptor-mediated events. The N-terminal RING domain of TRAF6 is required for its ability to signal by functioning as an E3 ubiquitin ligase, which catalyzes the synthesis of a polyubiquitin chain linked through Lys-63 (K63) residue in ubiquitin (Deng et al., 2000; Chen, 2005). This autoubiquitination of TRAF6 serves as a scaffold to recruit molecules required for the activation of kinase complexes such as transforming growth factor β–activated kinase 1 (TAK1) and I κB kinase (IKK; Lamothe et al., 2007a, 2008). The TAK1–TAB2 (or TAB3) complex that is activated potentially through TRAF6-dependent ubiquitination can phosphorylate IKKβ at Ser-177 and Ser-181 in the activation loop, leading to the activation of IKK and subsequently NF-κB (Shim et al., 2005). The activated TAK1 complex can also phosphorylate members of the MKK family, leading to the activation of JNK and p38 kinase

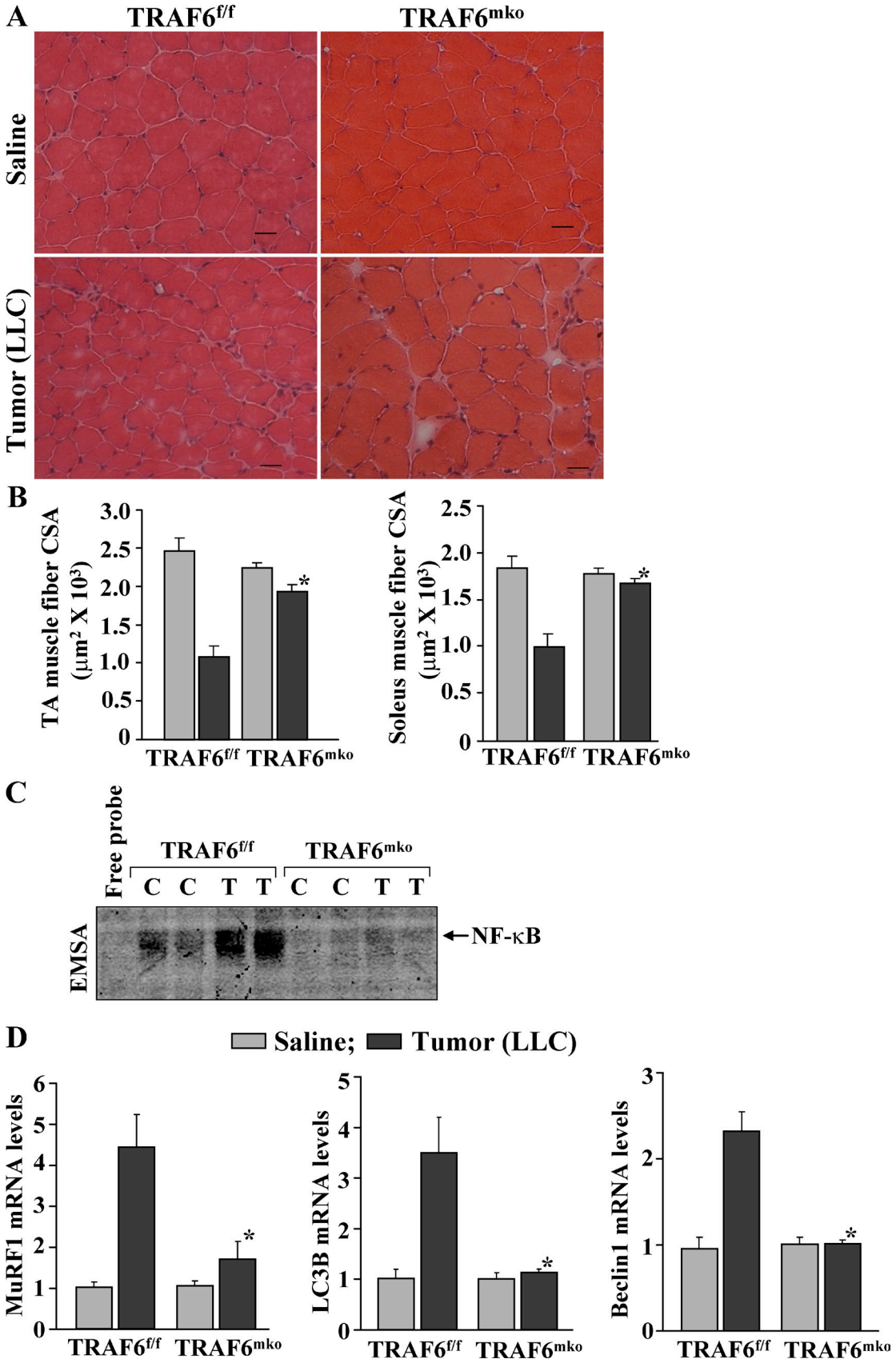

Figure 8. **Depletion of TRAF6 prevents tumor-induced muscle loss in mice.** LLC cells (2 × 10^6 cells in 100 µl saline) were injected in the left flank of TRAF6$^{f/f}$ and TRAF6^{mko} mice. Control mice received 100 µl of saline only. (A) TA muscles were isolated from control and tumor-bearing mice after 14 d and analyzed by staining with H&E. Representative photomicrographs presented here demonstrate that fiber CSA was preserved in TRAF6^{mko} mice (n = 7) compared with TRAF6$^{f/f}$ mice (n = 6). Bars, 20 µm. (B) Quantification of mean fiber CSA in TA and soleus muscle of TRAF6$^{f/f}$ and TRAF6^{mko} mice

(Moriguchi et al., 1996; Hanafusa et al., 1999; Wang et al., 2001). Interestingly, recent studies suggest that the activation of NF-κB in skeletal muscle up-regulates the expression of *MuRF1* in response to a variety of catabolic stimuli, including denervation and tumor growth (Cai et al., 2004; Mourkioti et al., 2006; Li et al., 2008; Mittal et al., 2010). Furthermore, there are also published studies suggesting that the p38 MAPK augments the expression of *MAFbx* in response to inflammatory cytokines and bacterial products (Li et al., 2005; Doyle et al., 2010). Because depletion of TRAF6 in skeletal muscle blocked the activation of both NF-κB and p38 MAPK in denervated skeletal muscle (Figs. 6 B and 7), it is likely that TRAF6 augments the expression of *MuRF1* and *MAFbx* through the activation of NF-κB and p38 MAPK, respectively, by stimulating the activity of TAK1 signalosome. The present study also provides novel evidence that the TWEAK-Fn14 dyad, a major regulator of denervation-induced skeletal muscle atrophy (Mittal et al., 2010), stimulates NF-κB activation through the recruitment of TRAF6 (Fig. 7, F and G).

In addition to the ubiquitin–proteasome system, the autophagy–lysosomal pathway has also been implicated in myofibril degradation in various atrophying conditions (Zhao et al., 2007; Sandri, 2010). Though it was initially considered as an important mechanism for removal of ubiquitinated protein aggregates and cytoplasmic organelles under the conditions of stress, recent evidence indicates that the activation of this pathway may also be a protective mechanism for muscle fibers in the conditions of atrophy (Zhao et al., 2007; Masiero et al., 2009; Sandri, 2010). Mitochondria are one of the most important organelles that undergo alterations in their content, shape, and function in conditions of muscle wasting (Figueiredo et al., 2008; Gamboa and Andrade, 2010). More recently, it has been found that the mitochondrial fission is a prerequisite for skeletal muscle atrophy in response to starvation or after overexpression of FoxO3, and that the autophagy–lysosomal system is the major mechanism for the removal of disintegrating mitochondria in these conditions (Romanello et al., 2010). The removal of leaky mitochondria, releasing pro-apoptotic factors such as cytochrome *c* and apoptosis-inducing factor, may protect cells by preventing activation of apoptosis (Hamacher-Brady et al., 2007; Mizushima and Levine, 2010; Romanello et al., 2010). The protective role of autophagy in skeletal muscle in catabolic conditions has also been highlighted by a recent study demonstrating that muscle-specific depletion of *Atg7*, an important component of the autophagy–lysosomal system, led to more severe myopathy in conditions of denervation (Masiero et al., 2009). This suggests that physiological autophagy may be required for muscle homeostasis, whereas its overstimulation in atrophying muscle may contribute to muscle proteolysis (Sandri, 2010). Intriguingly, our findings revealed that the inhibition of TRAF6 dramatically reduces mitochondrial disorganization and autophagosome formation (Fig. 5 D), as well as the activation of AMPK (Fig. 6 C), which is known to induce the expression of several autophagy-related genes (e.g., *LC3B* and *Bnip3*), and the E3 ligases *MuRF1* and *MAFbx* through the activation of FoxO3 transcription factor in skeletal muscle (Mammucari et al., 2007; Zhao et al., 2007; Romanello et al., 2010). Although mitochondrial fission has been suggested as an initial event to activate the autophagy pathway in skeletal muscle (Romanello et al., 2010), it has been recently demonstrated that TRAF6 causes the Lys-63–linked ubiquitination of Beclin1 (the mammalian homologue of yeast Atg6), which is essential for autophagosome formation in response to Toll-like receptor 4 (TLR4) signaling (Shi and Kehrl, 2010). Whether TRAF6 stimulates autophagosome formation through augmenting mitochondrial fission or if it directly regulates the expression and activity of the components of autophagy–lysosomal pathway is an area of research for future investigation.

We further investigated the contribution of TRAF6 toward muscle loss in cancer cachexia. Earlier studies have underlined the importance of inflammatory cytokines and tumor-derived factors as mediators of muscle loss in both animal models and advanced stages of cancer patients (Späte and Schulze, 2004; Argilés et al., 2005; Acharyya and Guttridge, 2007). Using transgenic mice expressing a constitutively active mutant of IKKβ, Cai et al. (2004) have previously demonstrated that the stimulation of the NF-κB pathway is sufficient to cause severe muscle loss in mice. Furthermore, their study also showed that muscle-specific overexpression of a super–repressor mutant of IκBα (inhibitor of NF-κB) significantly rescued muscle loss in response to tumor growth in mice (Cai et al., 2004). The present study provides convincing evidence that TRAF6 is an upstream regulator of LLC-induced muscle loss, NF-κB activation, and MuRF1 expression (Fig. 8). Interestingly, although NF-κB was found to regulate only the expression of *MuRF1* (Cai et al., 2004), our results indicate that TRAF6 also regulates the expression of autophagy-related genes (e.g., *LC3B* and *Beclin1*) in skeletal muscle of LLC-bearing animals (Fig. 8 D). Furthermore, the almost complete inhibition of LLC-induced expression of MuRF1, LC3B, and Beclin1 in skeletal muscle of TRAF6^{mko} mice compared with control mice is consistent with major amelioration in muscle atrophy in TRAF6^{mko} mice (Fig. 8, A and B).

The results of the present study suggest that though a significant inhibition in muscle atrophy was observed in models of both denervation and cancer cachexia, depletion of TRAF6 resulted in more drastic improvement in fiber CSA in skeletal muscle of LLC-bearing mice. A better rescuing effect in the cancer cachexia model compared with denervation could be attributed to the fact that cancer cachexia involves systemic inflammation, and proinflammatory cytokines are some of the most important mediators of muscle wasting in a cancer-bearing

after 14 d of tumor inoculation (n = 6 in each group). (C) Analysis of DNA-binding activity of NF-κB in TA muscle of control and LLC-inoculated TRAF6$^{f/f}$ (n = 4) and TRAF6^{mko} mice (n = 4). A representative EMSA gel is presented. (D) QRT-PCR analysis of mRNA levels of MuRF1, LC3B, and Beclin1 in TA muscle of TRAF6^{mko} and TRAF6$^{f/f}$ mice in response to LLC growth (n = 6 in each group). Error bars represent SD. *, $P < 0.01$ (values significantly different from TRAF6$^{f/f}$ mice inoculated with LLC).

host (Späte and Schulze, 2004; Argilés et al., 2005; Acharyya and Guttridge, 2007). Interestingly, several cytokines and tumor-derived factors require TRAF6 for the downstream activation of various cell signaling pathways such as NF-κB and MAPK, which were also activated in atrophying skeletal muscle (Chung et al., 2007; Lamothe et al., 2007b; Zapata et al., 2007). In contrast, denervation-induced muscle atrophy does not involve any systemic inflammation, though it was recently demonstrated that the TWEAK-Fn14 dyad is one of the important mediators of muscle loss under conditions of denervation (Jackman and Kandarian, 2004; Mittal et al., 2010). Although a significant amelioration in muscle atrophy was observed, the denervation-induced muscle loss was also not completely blunted in TWEAK-KO mice (Mittal et al., 2010). Therefore, it is possible that muscle atrophy in response to denervation also involves some other uncharacterized factors that function independent of TRAF6. Nevertheless, the present study provides strong evidence that TRAF6 is central regulator of major proteolytic pathways in different types of atrophy.

In summary, the broad benefits of TRAF6 blockade in skeletal muscle raise novel and exciting possibilities for therapeutic approaches for the treatment of muscle wasting diseases in humans.

Materials and methods

Animal protocols

A detailed protocol for the generation of floxed TRAF6 (TRAF6f/f) mice has been described previously (Kobayashi et al., 2003). C57BL6 and MCK-Cre (strain B6.FVB (129S4)-Tg (Ckmm-cre) 5 Khn/J) were obtained from Jackson ImmunoResearch Laboratories, Inc.

Sciatic denervation was performed by anesthetizing the mice with an intraperitoneal injection of Avertin (2,2,2,-tribromoethanol), shaving the left hind quarters, making a 0.5-cm incision ∼0.5 cm proximal to the knee on the lateral side of the right leg, separating the muscles at the fascia and lifting out the sciatic nerve with a surgical hook or forceps, removing a 2–3-mm piece of sciatic nerve, and finally closing the incision with surgical sutures.

Skeletal muscles from diabetic mice were provided by S. Srivastava (Diabetes and Obesity Center, University of Louisville, Louisville, KY). Diabetes was induced in 6-wk-old male C57BL6 mice by repeated low-dose STZ (55 mg/kg/d for six consecutive days, i.p.) treatment as described previously (Baba et al., 2009). Mice treated with vehicle only (0.05 mM sodium citrate, pH 4.5) served as controls. 1 wk after the last injection of STZ, blood was collected from the tail vein. All the STZ-injected mice had blood glucose >400 mg/dL. Mice were sacrificed 5 d after measuring the blood glucose levels. For the cancer cachexia model, LLC cells (2×10^6 cells in 100 µl saline; American Type Culture Collection) were injected subcutaneously into the flanks of 3-mo-old mice as described previously (Cai et al., 2004). Mice were weighed daily and sacrificed 14 d after injection to study muscle atrophy.

For studying NF-κB reporter gene activity, TA muscle was electroporated with pNF-κB-Luc (Takara Bio Inc.) and pRL-TK (Promega) following exactly same protocol as described previously (Mittal et al., 2010). All experimental protocols with mice were approved in advance by the Institutional Animal Care and Use Committee at University of Louisville.

Cell culture

C2C12 cells (a myoblastic cell line) were obtained from American Type Culture Collection. These cells were grown in DME containing 10% FBS. To induce differentiation, the cells were incubated in differentiation medium (2% horse serum in DME) for 96 h as described previously (Dogra et al., 2006, 2007). $TRAF6^{+/+}$ and $TRAF6^{-/-}$ MEFs were cultured in DME with 10% FBS. The cells were plated in 6-well tissue culture plates before treatment with recombinant TWEAK protein (R&D Systems) for measurement of DNA-binding activity of NF-κB by EMSA.

For NF-κB reporter gene assays, cells plated in 24-well tissue culture plates were transfected with pNF-κB-Luc plasmid (Takara Bio Inc.) using Effectene transfection reagent according to the protocol suggested by the manufacturer (QIAGEN). Transfection efficiency was controlled by cotransfection of cells with *Renilla* luciferase-encoding plasmid pRL-TK (Promega). After treatment with TWEAK, specimens were processed for luciferase expression using a Dual luciferase assay system with reporter lysis buffer per the manufacturer's instructions (Promega). Luciferase measurements were made using a luminometer (Berthold Detection Systems).

Histology and morphometric measurements

Hind limb muscles (soleus and TA) of mice were removed, frozen in isopentane cooled in liquid nitrogen, and sectioned in a microtome cryostat. For the assessment of tissue morphology or visualization of fibrosis, 10-µm-thick transverse sections of muscles were stained with H&E, and staining was visualized (without any imaging medium) at room temperature on a microscope (Eclipse TE 2000-U) using a Plan 10×, NA 0.25 PH1 DL or Plan-Fluor ELWD 20×, NA 0.45 Ph1 DM objective lens, a digital camera (Digital Sight DS-Fi1), and NIS Elements BR 3.00 software (all from Nikon). The images were stored as JPEG files, and image levels were equally adjusted using Photoshop CS2 software (Adobe). Fiber CSA was analyzed in H&E-stained soleus or TA muscle sections. For each muscle, the distribution of fiber CSA was calculated by analyzing 200–250 myofibers using NIS Elements BR 3.00 software (Nikon) as described previously (Mittal et al., 2010).

Transmission electron microscopy

Control and denervated TA muscle isolated from $TRAF6^{f/f}$ and $TRAF6^{mko}$ mice were fixed in 3% glutaraldehyde in 0.1 M cocodylate buffer overnight followed by fixing in 1% cocodylate-buffered osmium tetroxide. The tissue was dehydrated through a series of graded alcohols, and embedded in LX-112 plastic (Ladd Research Industries). Longitudinal sections (80 nm) were cut using an ultramicrotome (LKB) and stained with uranium acetate and lead citrate. Samples were analyzed using a transmission electron microscope (CM 12; Philips) operating at 60 kV. The pictures were captured at 8,800× magnification using a 3.2 megapixel digital camera (Sia-7C; Kodak) at room temperature. No imaging medium was used to visualize the pictures, and images were stored as JPEG files. Image levels were equally adjusted using Photoshop CS2 software.

RNA isolation and QRT-PCR

Isolation of total RNA and QRT-PCR were performed using a method that has been described previously (Dogra et al., 2006, 2007). In brief, RNA was extracted from homogenized tissues using TRIzol reagent (Invitrogen) and an RNeasy Mini kit (QIAGEN) according to the manufacturer's instructions. The quantification of mRNA expression was performed using the SYBR Green dye method on a 7300 Sequence Detection system (Applied Biosystems). 1 µg of purified RNA was used to synthesize first strand cDNA with a reverse transcription system using an oligo (dT) primer (Applied Biosystems) and Omniscript reverse transcription kit (QIAGEN). The first strand cDNA reaction (0.5 µl) was subjected to real-time PCR amplification using gene-specific primers. The sequence of the primers used is described in Table S1.

Approximately 25 µl of reaction volume was used for the real-time PCR assay that consisted of 2× (12.5 µl) Brilliant SYBR Green QPCR Master mix (Applied Biosystems), 400 nM of primers (0.5 µl each from the stock), 11 µl water, and 0.5 µl of template. The thermal conditions consisted of an initial denaturation at 95°C for 10 min followed by 40 cycles of denaturation at 95°C for 15 s, annealing and extension at 60°C for 1 min, and, for a final step, a melting curve of 95°C for 15 s, 60°C for 15 s, and 95°C for 15 s. All reactions were performed in duplicate to reduce variation. Data normalization was accomplished using the endogenous control (β-actin), and the normalized values were subjected to a $2^{-\Delta\Delta Ct}$ formula to calculate the fold change between the control and experimental groups.

Immunoprecipitation and Western blotting

Levels of different proteins in skeletal muscle were determined by performing immunoblotting as described previously (Kumar and Boriek, 2003; Mittal et al., 2010). In brief, tissues were washed with PBS and homogenized in Western blot lysis buffer A (50 mM Tris-Cl, pH 8.0, 200 mM NaCl, 50 mM NaF, 1 mM DTT, 1 mM sodium orthovanadate, 0.3% IGEPAL, and protease inhibitors). Approximately 100 µg of protein was resolved on each lane on 10–12% SDS-PAGE, electrotransferred onto nitrocellulose membrane, and probed using anti-TRAF6 (1:1,000; Millipore), anti-TRAF3 (1:1,000; Santa Cruz Biotechnology, Inc.), anti-TRAF4 (1:1,000; Santa Cruz Biotechnology, Inc.), anti-TAB1 (1:1,000; Cell Signaling Technology), anti-phospho p65 (1:500; Cell Signaling Technology), anti-p65 (1:1,000; Santa Cruz Biotechnology, Inc.), anti-phospho-JNK1/2

(1:1,000; Cell Signaling Technology), anti-JNK1/2 (1:1,000; Cell Signaling Technology), anti-phospho p38 (1:200; Cell Signaling Technology), anti-p38 (1:1,000; Cell Signaling Technology), anti–phospho-AMPK (1:500; Cell Signaling Technology), anti-AMPK (1:1,000; Cell Signaling Technology), anti-phospho Akt (1:500; Cell Signaling Technology), anti-Akt (1:500; Cell Signaling Technology), anti-mTOR (1:1,000; Cell Signaling Technology), anti–phospho-mTOR (1:1,000; Cell Signaling Technology), anti-LC3B (1:1,000; Cell Signaling Technology), anti–Beclin-1 (1:1,000; Cell Signaling Technology), anti-Fn14 (1:1,000; Cell Signaling Technology), MF-20 (1:1,000; Development Studies Hybridoma Bank, University of Iowa), anti-laminin (1:1,000; Sigma-Aldrich), anti-tropomyosin (1:2,000; Sigma-Aldrich), anti-troponin (1:1,000; Sigma-Aldrich), anti–sarcomeric α-actin (1:1,000; Sigma-Aldrich), anti-nNOS (1:500; Santa Cruz Biotechnology, Inc.), anti-dystrophin (1:200; Development Studies Hybridoma bank, University of Iowa), anti-tubulin (1:5,000; Cell Signaling Technology), and anti-MuRF1 (1:1,000; R&D Systems), then detected by chemiluminescence. The bands were quantified using ImageQuant TL software (GE Healthcare).

To study the auto-ubiquitination of TRAF6, muscle extract (400 µg protein) was incubated overnight with 1 µg anti-TRAF6 antibody (Millipore) in 600 µl of lysis buffer followed by addition of protein A–Sepharose beads and incubation at 4°C for additional 2 h. The beads were washed with lysis buffer and finally suspended in Laemmli's sample buffer (2×). Proteins were resolved on 10% SDS-PAGE gel and immunoblotted using anti-ubiquitin (1:1,000; Sigma-Aldrich).

Kinase assays

For JNK assay, 700 µg of muscle extract was immunoprecipitated with anti-JNK1 (1 µg per sample) overnight at 4°C. This was followed by addition of 30 µl of protein A–Sepharose beads. After 2 h, the beads were washed two times with lysis buffer A and two times with kinase assay buffer, then resuspended in 20 µl of kinase assay mixture containing 50 mM Hepes, pH 7.4, 20 mM $MgCl_2$, 2 mM dithiothreitol, 20 µCi of [γ-^{32}P]ATP, 10 µM of unlabeled ATP, and 2 µg of substrate glutathione S-transferase–c-Jun (amino acid residues 1–79). After incubation at 37°C for 20 min, the reaction was terminated by boiling with 10 µl of 4× Laemmli sample buffer for 3 min. Finally, the protein was resolved on a 10% polyacrylamide gel, then the gel was dried and the radioactive bands were visualized and quantitated by using a PhosphorImager and ImageQuant TL software (GE Healthcare).

The activity of Akt was assayed similar to JNK1 except that anti–Phospho-Akt conjugated Sepharose beads (Cell Signaling Technology) were used for immunoprecipitation, and GSK-3 fusion protein (Cell Signaling Technology) was used as a substrate in the reaction mixture. The activity of p38 kinase was measured using a nonradioactive p38 MAP Kinase Assay kit according a protocol suggested by the manufacturer (Cell Signaling Technology). Similarly, AMPK was assayed using a commercially available kit (MBL International).

EMSA

NF-κB activation in skeletal muscle was analyzed by EMSA as described previously (Kumar and Boriek, 2003), with some modifications. In brief, TA muscles isolated from mice were immediately frozen in liquid nitrogen and suspended at 1 mg of muscle weight per 18 µl of low-salt lysis buffer (10 mM Hepes, pH 7.9, 10 mM KCl, 1.5 mM $MgCl_2$, 0.1 mM EDTA, 0.1 mM EGTA, 1 mM dithiothreitol, 0.5 mM phenylmethylsulfonyl fluoride, 2.0 µg/ml leupeptin, 2.0 µg/ml aprotinin, and 0.5 mg/ml benzamidine) followed by mechanical grinding using a motor and pestle. Cells in the lysis buffer were allowed to swell on ice for 10 min followed immediately by three cycles of freeze/thaw lysis. The tubes containing the lysed muscle cells were then vortexed vigorously for 10 s, and the lysate was centrifuged for 30s at 14,000 rpm. The supernatant (cytoplasmic extract) was removed and saved at −70°C for further biochemical analyses. The nuclear pellet was resuspended in 4 µl of ice-cold high-salt nuclear extraction buffer (20 mM Hepes, pH 7.9, 420 mM NaCl, 1 mM EDTA, 1 mM EGTA, 150 mM $MgCl_2$, 25% glycerol, 1 mM dithiothreitol, 0.5 mM phenylmethylsulfonyl fluoride, 2.0 µg/ml leupeptin, 2.0 µg/ml aprotinin, and 0.5 mg/ml benzamidine) per milligram of original muscle weight and was incubated on ice for 30 min with intermittent vortexing. Samples were centrifuged for 5 min at 4°C, and the supernatant (nuclear extract) was either used immediately or stored at −80°C. The protein content was measured with the method of the Bio-Rad Laboratories protein assay reagent. EMSAs were performed by incubating 20 µg of nuclear extract with 16 fmol of the ^{32}P end-labeled NF-κB consensus oligonucleotides 5′-AGTTGAGGGGACTTTCCCAGGC-3′ (Promega) for 15 min at 37°C. The incubation mixture included 2–3 µg of poly dI.dC in a binding buffer (25 mM Hepes, pH 7.9, 0.5 mM EDTA, 0.5 mM dithiothreitol, 1% Nonidet P-40, 5% glycerol, and 50 mM NaCl). The DNA–protein complex thus formed was separated from free oligonucleotide on 7.5% native polyacrylamide gel using buffer containing 50 mM Tris, 200 mM glycine, pH 8.5, and 1 mM EDTA. The gel was dried, and the radioactive bands were visualized and quantitated by a PhosphorImager (GE Healthcare) using ImageQuant TL software.

Skeletal muscle functional analysis

The skeletal muscle force production in isometric contraction was performed as described previously (Li et al., 2009; Mittal et al., 2010). In brief, soleus muscle from control or denervated hind limb of mice was rapidly excised and placed in Krebs-Ringer solution. The muscle was mounted between a Fort25 force transducer (World Precision Instrumentation) and a micromanipulator device in a temperature-controlled myobath (World Precision Instrumentation). The muscle was positioned between platinum wire stimulating electrodes and stimulated to contract isometrically using electrical field stimulation (supramaximal voltage, 1.2-ms pulse duration) from a Grass S88 stimulator (Grass Technologies). In each experiment, muscle length was adjusted to optimize twitch force (optimal length, L_o). The muscle was rested for 15 min before the tetanic protocol was started. The output of the force transducer was recorded in computer using LABORATORY-TRAX-4 software. To evaluate a potentially different frequency response between groups, tetani were assessed by sequential stimulation at 25, 50, 75, 100, 150, 200, and 300 Hz with 100 s rest in between.

Statistical analysis

Results are expressed as mean ± SD. The Student's *t* test or analysis of variance was used to compare quantitative data populations with normal distributions and equal variance. A value of $P < 0.05$ was considered statistically significant unless otherwise specified.

Online supplemental material

Fig. S1 shows how the expression levels of various TRAFs change during differentiation of C2C12 myoblasts and how TRAF6 protein levels are affected in skeletal muscle of mice of different ages. Fig. S2 shows the breeding strategy used for generation of TRAF6$^{f/f}$ and TRAF6^{mko} mice and the initial characterization of skeletal muscle of 10-d- and 8-wk-old TRAF6$^{f/f}$ and TRAF6^{mko} mice. Fig. S3 examines the serum levels of CK and the proportion of slow- and fast-type fibers and ex vivo force production in soleus muscle of TRAF6$^{f/f}$ and TRAF6^{mko} mice. Table S1 describes the sequence of the primers used. Online supplemental material is available at http://www.jcb.org/cgi/content/full/jcb.201006098/DC1.

We thank Ms. Cathie Caple (Department of Anatomical Sciences and Neurobiology, University of Louisville School of Medicine, Louisville, KY) for her excellent technical help with electron microscopy and Dr. Sanjay Srivastava for providing muscle tissues from diabetic mice.

This study was supported by funding from National Institutes of Health (RO1 AG029623) and the University of Louisville Clinical and Translational Science Pilot Grant Program's Basic Award (CTSPGP) to A. Kumar. The authors declare that they have no conflict of interest.

Submitted: 16 June 2010
Accepted: 19 November 2010

References

Acharyya, S., and D.C. Guttridge. 2007. Cancer cachexia signaling pathways continue to emerge yet much still points to the proteasome. *Clin. Cancer Res.* 13:1356–1361. doi:10.1158/1078-0432.CCR-06-2307

Acharyya, S., K.J. Ladner, L.L. Nelsen, J. Damrauer, P.J. Reiser, S. Swoap, and D.C. Guttridge. 2004. Cancer cachexia is regulated by selective targeting of skeletal muscle gene products. *J. Clin. Invest.* 114:370–378.

Argilés, J.M., S. Busquets, and F.J. López-Soriano. 2005. The pivotal role of cytokines in muscle wasting during cancer. *Int. J. Biochem. Cell Biol.* 37:2036–2046. doi:10.1016/j.biocel.2005.03.014

Baba, S.P., O.A. Barski, Y. Ahmed, T.E. O'Toole, D.J. Conklin, A. Bhatnagar, and S. Srivastava. 2009. Reductive metabolism of AGE precursors: a metabolic route for preventing AGE accumulation in cardiovascular tissue. *Diabetes.* 58:2486–2497. doi:10.2337/db09-0375

Bodine, S.C., E. Latres, S. Baumhueter, V.K. Lai, L. Nunez, B.A. Clarke, W.T. Poueymirou, F.J. Panaro, E. Na, K. Dharmarajan, et al. 2001. Identification of ubiquitin ligases required for skeletal muscle atrophy. *Science.* 294:1704–1708. doi:10.1126/science.1065874

Brüning, J.C., M.D. Michael, J.N. Winnay, T. Hayashi, D. Hörsch, D. Accili, L.J. Goodyear, and C.R. Kahn. 1998. A muscle-specific insulin receptor knockout exhibits features of the metabolic syndrome of NIDDM

without altering glucose tolerance. *Mol. Cell.* 2:559–569. doi:10.1016/S1097-2765(00)80155-0

Cai, D., J.D. Frantz, N.E. Tawa Jr., P.A. Melendez, B.C. Oh, H.G. Lidov, P.O. Hasselgren, W.R. Frontera, J. Lee, D.J. Glass, and S.E. Shoelson. 2004. IKKbeta/NF-kappaB activation causes severe muscle wasting in mice. *Cell.* 119:285–298. doi:10.1016/j.cell.2004.09.027

Cao, P.R., H.J. Kim, and S.H. Lecker. 2005. Ubiquitin-protein ligases in muscle wasting. *Int. J. Biochem. Cell Biol.* 37:2088–2097. doi:10.1016/j.biocel.2004.11.010

Chen, Z.J. 2005. Ubiquitin signalling in the NF-kappaB pathway. *Nat. Cell Biol.* 7:758–765. doi:10.1038/ncb0805-758

Chung, J.Y., M. Lu, Q. Yin, S.C. Lin, and H. Wu. 2007. Molecular basis for the unique specificity of TRAF6. *Adv. Exp. Med. Biol.* 597:122–130. doi:10.1007/978-0-387-70630-6_10

Clarke, B.A., D. Drujan, M.S. Willis, L.O. Murphy, R.A. Corpina, E. Burova, S.V. Rakhilin, T.N. Stitt, C. Patterson, E. Latres, and D.J. Glass. 2007. The E3 Ligase MuRF1 degrades myosin heavy chain protein in dexamethasone-treated skeletal muscle. *Cell Metab.* 6:376–385. doi:10.1016/j.cmet.2007.09.009

Cohen, S., J.J. Brault, S.P. Gygi, D.J. Glass, D.M. Valenzuela, C. Gartner, E. Latres, and A.L. Goldberg. 2009. During muscle atrophy, thick, but not thin, filament components are degraded by MuRF1-dependent ubiquitylation. *J. Cell Biol.* 185:1083–1095. doi:10.1083/jcb.200901052

Criollo, A., L. Senovilla, H. Authier, M.C. Maiuri, E. Morselli, I. Vitale, O. Kepp, E. Tasdemir, L. Galluzzi, S. Shen, et al. 2010a. The IKK complex contributes to the induction of autophagy. *EMBO J.* 29:619–631. doi:10.1038/emboj.2009.364

Criollo, A., L. Senovilla, H. Authier, M.C. Maiuri, E. Morselli, I. Vitale, O. Kepp, E. Tasdemir, L. Galluzzi, S. Shen, et al. 2010b. IKK connects autophagy to major stress pathways. *Autophagy.* 6:189–191. doi:10.4161/auto.6.1.10818

Deng, L., C. Wang, E. Spencer, L. Yang, A. Braun, J. You, C. Slaughter, C. Pickart, and Z.J. Chen. 2000. Activation of the IkappaB kinase complex by TRAF6 requires a dimeric ubiquitin-conjugating enzyme complex and a unique polyubiquitin chain. *Cell.* 103:351–361. doi:10.1016/S0092-8674(00)00126-4

Dogra, C., H. Changotra, S. Mohan, and A. Kumar. 2006. Tumor necrosis factor-like weak inducer of apoptosis inhibits skeletal myogenesis through sustained activation of nuclear factor-kappaB and degradation of MyoD protein. *J. Biol. Chem.* 281:10327–10336. doi:10.1074/jbc.M511131200

Dogra, C., H. Changotra, N. Wedhas, X. Qin, J.E. Wergedal, and A. Kumar. 2007. TNF-related weak inducer of apoptosis (TWEAK) is a potent skeletal muscle-wasting cytokine. *FASEB J.* 21:1857–1869. doi:10.1096/fj.06-7537com

Doyle, A., G. Zhang, E.A. Abdel Fattah, N. Tony Eissa, and Y.P. Li. 2010. Toll-like receptor 4 mediates lipopolysaccharide-induced muscle catabolism via coordinate activation of ubiquitin-proteasome and autophagy-lysosome pathways. *FASEB J.* In press.

Figueiredo, P.A., M.P. Mota, H.J. Appell, and J.A. Duarte. 2008. The role of mitochondria in aging of skeletal muscle. *Biogerontology.* 9:67–84. doi:10.1007/s10522-007-9121-7

Gamboa, J.L., and F.H. Andrade. 2010. Mitochondrial content and distribution changes specific to mouse diaphragm after chronic normobaric hypoxia. *Am. J. Physiol. Regul. Integr. Comp. Physiol.* 298:R575–R583.

Glass, D.J. 2003. Molecular mechanisms modulating muscle mass. *Trends Mol. Med.* 9:344–350. doi:10.1016/S1471-4914(03)00138-2

Glass, D.J. 2005. Skeletal muscle hypertrophy and atrophy signaling pathways. *Int. J. Biochem. Cell Biol.* 37:1974–1984.

Glass, D.J. 2010. Signaling pathways perturbing muscle mass. *Curr. Opin. Clin. Nutr. Metab. Care.* 13:225–229. doi:10.1097/MCO.0b013e32833862df

Gomes, M.D., S.H. Lecker, R.T. Jagoe, A. Navon, and A.L. Goldberg. 2001. Atrogin-1, a muscle-specific F-box protein highly expressed during muscle atrophy. *Proc. Natl. Acad. Sci. USA.* 98:14440–14445. doi:10.1073/pnas.251541198

Hamacher-Brady, A., N.R. Brady, S.E. Logue, M.R. Sayen, M. Jinno, L.A. Kirshenbaum, R.A. Gottlieb, and A.B. Gustafsson. 2007. Response to myocardial ischemia/reperfusion injury involves Bnip3 and autophagy. *Cell Death Differ.* 14:146–157. doi:10.1038/sj.cdd.4401936

Hanafusa, H., J. Ninomiya-Tsuji, N. Masuyama, M. Nishita, J. Fujisawa, H. Shibuya, K. Matsumoto, and E. Nishida. 1999. Involvement of the p38 mitogen-activated protein kinase pathway in transforming growth factor-beta-induced gene expression. *J. Biol. Chem.* 274:27161–27167. doi:10.1074/jbc.274.38.27161

Jackman, R.W., and S.C. Kandarian. 2004. The molecular basis of skeletal muscle atrophy. *Am. J. Physiol. Cell Physiol.* 287:C834–C843. doi:10.1152/ajpcell.00579.2003

Kandarian, S.C., and E.J. Stevenson. 2002. Molecular events in skeletal muscle during disuse atrophy. *Exerc. Sport Sci. Rev.* 30:111–116. doi:10.1097/00003677-200207000-00004

Kedar, V., H. McDonough, R. Arya, H.H. Li, H.A. Rockman, and C. Patterson. 2004. Muscle-specific RING finger 1 is a bona fide ubiquitin ligase that degrades cardiac troponin I. *Proc. Natl. Acad. Sci. USA.* 101:18135–18140. doi:10.1073/pnas.0404341102

Kobayashi, T., P.T. Walsh, M.C. Walsh, K.M. Speirs, E. Chiffoleau, C.G. King, W.W. Hancock, J.H. Caamano, C.A. Hunter, P. Scott, et al. 2003. TRAF6 is a critical factor for dendritic cell maturation and development. *Immunity.* 19:353–363. doi:10.1016/S1074-7613(03)00230-9

Krawiec, B.J., G.J. Nystrom, R.A. Frost, L.S. Jefferson, and C.H. Lang. 2007. AMP-activated protein kinase agonists increase mRNA content of the muscle-specific ubiquitin ligases MAFbx and MuRF1 in C2C12 cells. *Am. J. Physiol. Endocrinol. Metab.* 292:E1555–E1567. doi:10.1152/ajpendo.00622.2006

Kumar, A., and A.M. Boriek. 2003. Mechanical stress activates the nuclear factor-kappaB pathway in skeletal muscle fibers: a possible role in Duchenne muscular dystrophy. *FASEB J.* 17:386–396. doi:10.1096/fj.02-0542com

Kumar, A., Y. Takada, A.M. Boriek, and B.B. Aggarwal. 2004. Nuclear factor-kappaB: its role in health and disease. *J. Mol. Med.* 82:434–448. doi:10.1007/s00109-004-0555-y

Lamothe, B., A. Besse, A.D. Campos, W.K. Webster, H. Wu, and B.G. Darnay. 2007a. Site-specific Lys-63-linked tumor necrosis factor receptor-associated factor 6 auto-ubiquitination is a critical determinant of I kappa B kinase activation. *J. Biol. Chem.* 282:4102–4112. doi:10.1074/jbc.M609503200

Lamothe, B., W.K. Webster, A. Gopinathan, A. Besse, A.D. Campos, and B.G. Darnay. 2007b. TRAF6 ubiquitin ligase is essential for RANKL signaling and osteoclast differentiation. *Biochem. Biophys. Res. Commun.* 359:1044–1049. doi:10.1016/j.bbrc.2007.06.017

Lamothe, B., A.D. Campos, W.K. Webster, A. Gopinathan, L. Hur, and B.G. Darnay. 2008. The RING domain and first zinc finger of TRAF6 coordinate signaling by interleukin-1, lipopolysaccharide, and RANKL. *J. Biol. Chem.* 283:24871–24880. doi:10.1074/jbc.M802749200

Lecker, S.H., A.L. Goldberg, and W.E. Mitch. 2006. Protein degradation by the ubiquitin-proteasome pathway in normal and disease states. *J. Am. Soc. Nephrol.* 17:1807–1819. doi:10.1681/ASN.2006010083

Lee, N.K., and S.Y. Lee. 2002. Modulation of life and death by the tumor necrosis factor receptor-associated factors (TRAFs). *J. Biochem. Mol. Biol.* 35:61–66.

Li, Y.P., Y. Chen, J. John, J. Moylan, B. Jin, D.L. Mann, and M.B. Reid. 2005. TNF-alpha acts via p38 MAPK to stimulate expression of the ubiquitin ligase atrogin1/MAFbx in skeletal muscle. *FASEB J.* 19:362–370. doi:10.1096/fj.04-2364com

Li, H., S. Malhotra, and A. Kumar. 2008. Nuclear factor-kappa B signaling in skeletal muscle atrophy. *J. Mol. Med.* 86:1113–1126. doi:10.1007/s00109-008-0373-8

Li, H., A. Mittal, D.Y. Makonchuk, S. Bhatnagar, and A. Kumar. 2009. Matrix metalloproteinase-9 inhibition ameliorates pathogenesis and improves skeletal muscle regeneration in muscular dystrophy. *Hum. Mol. Genet.* 18:2584–2598. doi:10.1093/hmg/ddp191

Lomaga, M.A., W.C. Yeh, I. Sarosi, G.S. Duncan, C. Furlonger, A. Ho, S. Morony, C. Capparelli, G. Van, S. Kaufman, et al. 1999. TRAF6 deficiency results in osteopetrosis and defective interleukin-1, CD40, and LPS signaling. *Genes Dev.* 13:1015–1024. doi:10.1101/gad.13.8.1015

Mammucari, C., G. Milan, V. Romanello, E. Masiero, R. Rudolf, P. Del Piccolo, S.J. Burden, R. Di Lisi, C. Sandri, J. Zhao, et al. 2007. FoxO3 controls autophagy in skeletal muscle in vivo. *Cell Metab.* 6:458–471. doi:10.1016/j.cmet.2007.11.001

Masiero, E., L. Agatea, C. Mammucari, B. Blaauw, E. Loro, M. Komatsu, D. Metzger, C. Reggiani, S. Schiaffino, and M. Sandri. 2009. Autophagy is required to maintain muscle mass. *Cell Metab.* 10:507–515. doi:10.1016/j.cmet.2009.10.008

Matsuda, R., D. Spector, and R.C. Strohman. 1984. Denervated skeletal muscle displays discoordinate regulation for the synthesis of several myofibrillar proteins. *Proc. Natl. Acad. Sci. USA.* 81:1122–1125. doi:10.1073/pnas.81.4.1122

Meley, D., C. Bauvy, J.H. Houben-Weerts, P.F. Dubbelhuis, M.T. Helmond, P. Codogno, and A.J. Meijer. 2006. AMP-activated protein kinase and the regulation of autophagic proteolysis. *J. Biol. Chem.* 281:34870–34879. doi:10.1074/jbc.M605488200

Mittal, A., S. Bhatnagar, A. Kumar, E. Lach-Trifilieff, S. Wauters, H. Li, D.Y. Makonchuk, D.J. Glass, and A. Kumar. 2010. The TWEAK-Fn14 system is a critical regulator of denervation-induced skeletal muscle atrophy in mice. *J. Cell Biol.* 188:833–849. doi:10.1083/jcb.200909117

Mizushima, N., and B. Levine. 2010. Autophagy in mammalian development and differentiation. *Nat. Cell Biol.* 12:823–830. doi:10.1038/ncb0910-823

Moriguchi, T., N. Kuroyanagi, K. Yamaguchi, Y. Gotoh, K. Irie, T. Kano, K. Shirakabe, Y. Muro, H. Shibuya, K. Matsumoto, et al. 1996. A novel

kinase cascade mediated by mitogen-activated protein kinase kinase 6 and MKK3. *J. Biol. Chem.* 271:13675–13679. doi:10.1074/jbc.271.23.13675

Moscat, J., M.T. Diaz-Meco, \and M.W. Wooten. 2007. Signal integration and diversification through the p62 scaffold protein. *Trends Biochem. Sci.* 32:95–100. doi:10.1016/j.tibs.2006.12.002

Mourkioti, F., P. Kratsios, T. Luedde, Y.H. Song, P. Delafontaine, R. Adami, V. Parente, R. Bottinelli, M. Pasparakis, and N. Rosenthal. 2006. Targeted ablation of IKK2 improves skeletal muscle strength, maintains mass, and promotes regeneration. *J. Clin. Invest.* 116:2945–2954. doi:10.1172/JCI28721

Mukhopadhyay, D., and H. Riezman. 2007. Proteasome-independent functions of ubiquitin in endocytosis and signaling. *Science.* 315:201–205. doi:10.1126/science.1127085

Naito, A., S. Azuma, S. Tanaka, T. Miyazaki, S. Takaki, K. Takatsu, K. Nakao, K. Nakamura, M. Katsuki, T. Yamamoto, and J. Inoue. 1999. Severe osteopetrosis, defective interleukin-1 signalling and lymph node organogenesis in TRAF6-deficient mice. *Genes Cells.* 4:353–362. doi:10.1046/j.1365-2443.1999.00265.x

Nakamura, K., A.J. Kimple, D.P. Siderovski, and G.L. Johnson. 2010. PB1 domain interaction of p62/sequestosome 1 and MEKK3 regulates NF-kappaB activation. *J. Biol. Chem.* 285:2077–2089. doi:10.1074/jbc.M109.065102

Pickart, C.M. 2001. Mechanisms underlying ubiquitination. *Annu. Rev. Biochem.* 70:503–533. doi:10.1146/annurev.biochem.70.1.503

Romanello, V., E. Guadagnin, L. Gomes, I. Roder, C. Sandri, Y. Petersen, G. Milan, E. Masiero, P. Del Piccolo, M. Foretz, et al. 2010. Mitochondrial fission and remodelling contributes to muscle atrophy. *EMBO J.* 29:1774–1785. doi:10.1038/emboj.2010.60

Sandri, M. 2010. Autophagy in skeletal muscle. *FEBS Lett.* 584:1411–1416. doi:10.1016/j.febslet.2010.01.056

Seibenhener, M.L., J.R. Babu, T. Geetha, H.C. Wong, N.R. Krishna, and M.W. Wooten. 2004. Sequestosome 1/p62 is a polyubiquitin chain binding protein involved in ubiquitin proteasome degradation. *Mol. Cell. Biol.* 24:8055–8068. doi:10.1128/MCB.24.18.8055-8068.2004

Shi, C.S., and J.H. Kehrl. 2010. TRAF6 and A20 regulate lysine 63-linked ubiquitination of Beclin-1 to control TLR4-induced autophagy. *Sci. Signal.* 3:ra42. doi:10.1126/scisignal.2000751

Shim, J.H., C. Xiao, A.E. Paschal, S.T. Bailey, P. Rao, M.S. Hayden, K.Y. Lee, C. Bussey, M. Steckel, N. Tanaka, et al. 2005. TAK1, but not TAB1 or TAB2, plays an essential role in multiple signaling pathways in vivo. *Genes Dev.* 19:2668–2681. doi:10.1101/gad.1360605

Solomon, V., and A.L. Goldberg. 1996. Importance of the ATP-ubiquitin-proteasome pathway in the degradation of soluble and myofibrillar proteins in rabbit muscle extracts. *J. Biol. Chem.* 271:26690–26697. doi:10.1074/jbc.271.41.25240

Späte, U., and P.C. Schulze. 2004. Proinflammatory cytokines and skeletal muscle. *Curr. Opin. Clin. Nutr. Metab. Care.* 7:265–269. doi:10.1097/00075197-200405000-00005

Supinski, G.S., X. Ji, and L.A. Callahan. 2009. The JNK MAP kinase pathway contributes to the development of endotoxin-induced diaphragm caspase activation. *Am. J. Physiol. Regul. Integr. Comp. Physiol.* 297:R825–R834.

Tintignac, L.A., J. Lagirand, S. Batonnet, V. Sirri, M.P. Leibovitch, and S.A. Leibovitch. 2005. Degradation of MyoD mediated by the SCF (MAFbx) ubiquitin ligase. *J. Biol. Chem.* 280:2847–2856. doi:10.1074/jbc.M411346200

Wang, C., L. Deng, M. Hong, G.R. Akkaraju, J. Inoue, and Z.J. Chen. 2001. TAK1 is a ubiquitin-dependent kinase of MKK and IKK. *Nature.* 412:346–351. doi:10.1038/35085597

Wooten, M.W., T. Geetha, M.L. Seibenhener, J.R. Babu, M.T. Diaz-Meco, and J. Moscat. 2005. The p62 scaffold regulates nerve growth factor-induced NF-kappaB activation by influencing TRAF6 polyubiquitination. *J. Biol. Chem.* 280:35625–35629. doi:10.1074/jbc.C500237200

Yamashita, M., K. Fatyol, C. Jin, X. Wang, Z. Liu, and Y.E. Zhang. 2008. TRAF6 mediates Smad-independent activation of JNK and p38 by TGF-beta. *Mol. Cell.* 31:918–924. doi:10.1016/j.molcel.2008.09.002

Yang, W.L., J. Wang, C.H. Chan, S.W. Lee, A.D. Campos, B. Lamothe, L. Hur, B.C. Grabiner, X. Lin, B.G. Darnay, and H.K. Lin. 2009. The E3 ligase TRAF6 regulates Akt ubiquitination and activation. *Science.* 325:1134–1138. doi:10.1126/science.1175065

Zapata, J.M., S. Lefebvre, and J.C. Reed. 2007. Targeting TRAfs for therapeutic intervention. *Adv. Exp. Med. Biol.* 597:188–201. doi:10.1007/978-0-387-70630-6_15

Zhao, J., J.J. Brault, A. Schild, P. Cao, M. Sandri, S. Schiaffino, S.H. Lecker, and A.L. Goldberg. 2007. FoxO3 coordinately activates protein degradation by the autophagic/lysosomal and proteasomal pathways in atrophying muscle cells. *Cell Metab.* 6:472–483. doi:10.1016/j.cmet.2007.11.004